

Testing Hypotheses in Particle Physics: Plots of p_0 Versus p_1

Luc Demortier[†], Louis Lyons[‡]

[†]*Laboratory of Experimental High Energy Physics
The Rockefeller University, New York, NY 10065, USA*

[‡]*Blackett Laboratory
Imperial College, London SW7 2BW, UK*

August 27, 2014

Abstract

For situations where we are trying to decide which of two hypotheses H_0 and H_1 provides a better description of some data, we discuss the usefulness of plots of p_0 versus p_1 , where p_i is the p -value for testing H_i . They provide an interesting way of understanding the difference between the standard way of excluding H_1 and the CL_s approach; the Punzi definition of sensitivity; the relationship between p -values and likelihood ratios; and the probability of observing misleading evidence. They also help illustrate the Law of the Iterated Logarithm and the Jeffreys-Lindley paradox.

1 Introduction

Very often in particle physics we try to see whether some data are consistent with the standard model (SM) with the currently known particles (call this hypothesis H_0), or whether it favors a more or less specific form of new physics in addition to the SM background (H_1). This could be, for example, a particular form of leptoquark with a well-defined mass; or with a mass in some range (e.g. 50 to 1000 GeV). In the first case there are no free parameters and H_1 is described as being ‘simple’, while in the latter case, because of the unspecified leptoquark mass, H_1 is ‘composite’.

If the only free parameter in the alternative hypothesis H_1 is the mass of some new particle, we can test each mass in H_1 separately against H_0 , in which case we are comparing two simple hypotheses. However, the ensemble of different possible masses in the overall procedure (known as a ‘raster scan’ [1]) makes H_1 composite. Insight into this type of situation is facilitated by two-dimensional ‘ p -value plots’, where the significance of possible observations under the null hypothesis is plotted against their significance under various values of the free parameter in the alternative hypothesis [2]. The purpose of this article is to use such plots to explore various aspects of hypothesis testing in particle physics¹.

¹In this article we concentrate on hypothesis testing procedures pertaining to discovery claims in search experiments (not necessarily in particle physics). We do not consider other uses of hypothesis testing, such as in particle physics event selection for instance. The desiderata are slightly different.

We begin in section 2 by recapitulating the types of hypothesis testing familiar from the statistics literature, and contrasting these with the practice in particle physics. Section 3 introduces p -value plots and uses them to discuss the CL_s criterion, upper limits, fixed-hypothesis contours, and the Punzi definition of sensitivity. The probabilities for observations to fall into various regions of a p -value plot are derived in section 4, together with the error rates and power of a particle physics test. Likelihood ratios form the subject of section 5, where they are compared to p -values and used to plot contours and to compute probabilities of misleading evidence. Two famous p -value puzzles are described in section 6. Section 7 contains remarks on the effect of nuisance parameters, and our conclusions and recommendations appear in section 8. An appendix provides technical details about the relationship between CL_s and Bayesian upper limits.

2 Types and outcomes of hypothesis testing

When using observed data to test one or more hypotheses, the first step is to design a test statistic T that summarizes the relevant properties of the data. The observed value t of T is then referred to its probability distribution under each specified hypothesis in order to assess evidence. The form of the test statistic depends on the type of test one is interested in.

Comparisons of data with *a single hypothesis* are performed via ‘goodness of fit’ tests. An example of this is the χ^2 test, which generally requires the data to be binned, and where T is equal to the sum of the squares of the numbers of standard deviations between observed and expected bin contents. Another well-known technique, which does not require binning, is the Kolmogorov-Smirnov test, where T is constructed from the expected and observed cumulative distributions of the data. There are many other techniques [3, 4]. The outcome of a goodness-of-fit test is either ‘Reject’ or ‘Fail to reject’ the hypothesis of interest.

Comparison of the data with more than one hypothesis in order to decide which is favored is known as ‘hypothesis testing’. If there are *just two simple hypotheses* H_0 and H_1 , the appropriate framework is Neyman-Pearson hypothesis testing. The optimal test statistic T in this case is the likelihood ratio for the two hypotheses, or a one-to-one function of it ². The outcome of a Neyman-Pearson test is either ‘Reject H_0 and accept H_1 ,’ or ‘Accept H_0 and reject H_1 .’

In particle physics it often happens that we need to consider additional possible outcomes of a test. In the leptoquark example, an observed signal could be due to something entirely different from a leptoquark: some new physics that we did not anticipate, or a systematic bias that we did not model. Hence we may need to reject both H_0 and H_1 in favor of a third, unspecified hypothesis. On the other hand it may also happen that the data sample does not allow us to reject either H_0 or H_1 [5]. This leads to the formulation of a ‘double test’ of two hypotheses H_0 and H_1 , which are independently tested, resulting in four possible outcomes:

1. Fail to reject H_0 , and reject H_1 . This is referred to as ‘ H_1 excluded,’ and in a frequentist approach the rejection of H_1 is valid at some level of confidence, typically 95%.
2. Fail to reject H_0 and fail to reject H_1 (‘No decision’).

²In the case of a counting experiment, the number of observed counts n is typically a one-to-one function of the likelihood ratio for the ‘signal+background’ and ‘background-only’ hypotheses (H_1 and H_0 respectively).

3. Reject H_0 , and fail to reject H_1 . This corresponds to ‘Discovery of H_1 .’ In a frequentist approach the rejection of H_0 is valid at some confidence level, which in particle physics is usually much higher than the confidence level used for excluding H_1 . Typically the significance level, defined as one minus the confidence level, is set at 2.87×10^{-7} for rejecting H_0 . This is the area under a Gaussian tail, starting five standard deviations away from the mean.
4. Reject both H_0 and H_1 .

Often a likelihood ratio is used as the test statistic T for a double test.

For given H_0 and for fixed values of the parameters in H_1 , we can plot the probability density functions (pdf’s) of T , assuming (a) that hypothesis H_0 is true, or (b) that H_1 is true. Three possible situations are shown in figure 1. In (a), the two hypotheses are hard to distinguish as the pdf’s lie almost on top of each other; this could happen if H_1 involved a new particle that was only very weakly produced. In (b), the pdf’s still overlap to some extent, but distinguishing between the two hypotheses may be possible for some data sets. Finally (c) shows a situation where it is relatively easy to choose between the hypotheses.

3 p-Values

The degree to which the data are unexpected for a given hypothesis can be quantified via the p -value. This is the fractional area in the tail of the relevant pdf, with a value of t at least as extreme as that in the data. In tests involving two hypotheses, it is conventional to use the one-sided tail in the direction of the other hypothesis. For the examples shown in figure 1, this corresponds to p_0 being the right-hand tail of H_0 and p_1 the left-hand tail of H_1 .³ In the extreme case where H_0 and H_1 coincide (and where t is continuous rather than discrete), $p_0 + p_1 = 1$.

3.1 Regions in the (p_0, p_1) plane

Figure 2 contains a plot of p_0 versus p_1 , with the regions for which the double test either rejects H_0 or fails to reject it; these depend solely on p_0 . In the diagram, the critical value α_0 for p_0 is shown at 0.05; this value is chosen here for clear visibility on the plot, rather than as a realistic choice.

In particle physics, when we fail to reject H_0 , we want to see further whether we can exclude H_1 . Although not as exciting as discovery, exclusion can be useful from a theoretical point of view and also for the purpose of planning the next measurement. The most famous example is the Michelson-Morley experiment, which excluded any significant velocity of the earth with respect to the aether and led to the demise of the aether theory. In figure 2, the region $p_1 \leq \alpha_1$ is used for excluding H_1 . The critical value α_1 is usually chosen to be larger than the p_0 cut-off α_0 ; 0.05 is a typical value. In the figure α_1 is shown at 0.10.

³In this paper we do not consider problems in which it is desired to reject H_0 when the data statistic t falls in the extreme left-tail of the H_0 pdf (see figure 1), or to reject H_1 when t is very large. Our p -values are one-sided and would therefore be close to unity in these cases.

If p_0 and p_1 fall in the large rectangle at the top right of the plot ($p_0 > \alpha_0$ and $p_1 > \alpha_1$), we claim neither discovery of H_1 nor its exclusion: this is the no-decision region. The small rectangle near the origin corresponds to both p -values being below their cut-offs, and the data are unlikely under either hypothesis. It could correspond to the new physics occurring, but at a lower than expected rate.

3.2 The CL_s criterion

An alternative approach for exclusion of H_1 is the CL_s criterion [6]. Because exclusion levels are chosen to have modest values (say 95%), there is substantial probability (5%) that H_1 will be excluded even when the experiment has little sensitivity for distinguishing H_1 from H_0 (the situation shown in figure 1(a)). Although professional statisticians are not worried about this, in particle physics it is regarded as unsatisfactory. To protect against this, instead of rejecting H_1 on the basis of p_1 being small, a cut is made on

$$CL_s \equiv \frac{p_1}{1 - p_0}, \quad (1)$$

i.e. on the ratio of the left-hand tails of the H_0 and H_1 pdf's. Thus if the pdf's are almost indistinguishable, the ratio will be close to unity, and H_1 will not be excluded. In figure 2, the region below the dashed line referred to as ' CL_s ' shows where H_1 would be excluded. This is to be compared to the larger region below the horizontal line for the more conventional exclusion based on p_1 alone. The CL_s approach can thus be regarded as a conservative modification of the exact frequentist method; conservatism is the price to pay for the protection CL_s provides against exclusion when there is little or no sensitivity to H_1 .

3.3 Upper limits

As pointed out in the introduction, the pdf of H_1 often contains one or more parameters of interest whose values are not specified (e.g. the mass of a new particle, the cross section of a new process, etc.). It is then useful to determine the subset of H_1 parameter space where, with significance threshold α_1 , each parameter value is excluded by the observations. In the frequentist paradigm, the complement of this subset is a $CL = 1 - \alpha_1$ confidence region.

For a simple and common example consider the case where the pdf of the data depends on the cross section μ of a new physics process: then $\mu > 0$ if the process is present in the data (H_1 true), and $\mu = 0$ otherwise (H_0 true). Suppose that the test statistic T is stochastically increasing with μ , meaning that for fixed T , increasing μ reduces the p -value p_1 . Then the set of μ values that *cannot* be excluded by the observations has an upper limit, and that upper limit has confidence level $1 - \alpha_1$.

If instead of rejecting H_1 with the standard frequentist criterion $p_1 \leq \alpha_1$, we use the CL_s criterion $CL_s \leq \alpha_1$, the above procedure yields a CL_s upper limit for μ , which is higher (i.e. weaker) than the standard frequentist upper limit.

In the previous example suppose that, instead of a cross section, μ is a location parameter for the test statistic t . More precisely, suppose that the pdf of t is of the form $f(t - \mu)$, with f a continuous distribution. Then it can be shown that the upper limit using CL_s at the $1 - \alpha_1$ level coincides exactly with the credibility $1 - \alpha_1$ Bayesian upper limit obtained by

assuming a uniform prior for μ under H_1 (i.e., a prior that is a non-zero constant for $\mu > 0$, and zero elsewhere). This result extends to the discrete case where t is a Poisson-distributed event count with mean μ (see Appendix A).

3.4 Fixed-hypothesis contours in the $(\mathbf{p}_0, \mathbf{p}_1)$ plane.

If we keep the hypotheses H_0 and H_1 fixed, but vary the observed data statistic t , the point $(p_{0,\text{obs}}, p_{1,\text{obs}})$ will trace a contour in the (p_0, p_1) plane. In general this contour depends on the particular characteristics of each hypothesis, but useful simplifications may occur when the pdf of the test statistic is translation-invariant or enjoys other symmetries. Here we give four examples based on the pdf's shown in figure 3. The corresponding contours⁴ are drawn in figure 4 and assume that the test is of the basic form $H_0 : \mu = \mu_0$ versus $H_1 : \mu = \mu_1$, with $\mu_1 > \mu_0$, and that the test statistic is T ⁵. The parameter μ could be related to the strength of a possible signal for a new particle with unknown mass. Increasing separation between μ_0 and μ_1 could then correspond to increasing amount of data; fixed amount of data and fixed particle mass, but increasing cross section; fixed amount of data and varying particle mass, with the cross section depending on the mass in a known way (i.e. raster scan).

Example 1: μ is the mean of a Gaussian distribution of known width σ :

$$T \sim \frac{e^{-\frac{1}{2}\left(\frac{t-\mu}{\sigma}\right)^2}}{\sqrt{2\pi}\sigma}. \quad (2)$$

In this case the fixed-hypothesis contours only depend on $\Delta\mu/\sigma$, with $\Delta\mu \equiv \mu_1 - \mu_0$, and have the form:

$$\text{erf}^{-1}(1 - 2p_1) + \text{erf}^{-1}(1 - 2p_0) = \frac{\Delta\mu}{\sqrt{2}\sigma}. \quad (3)$$

Figure 4(a) shows three examples of this, with $\Delta\mu/\sigma = 0$ (when the locus is the diagonal line $p_0 + p_1 = 1$), 1.67 and 3.33. As $\Delta\mu/\sigma$ increases, the curves pass closer to the origin.

Example 2: μ is the mode of a Cauchy distribution with known half-width at half-height γ :

$$T \sim \frac{\gamma}{\pi [\gamma^2 + (t - \mu)^2]}. \quad (4)$$

The contours have a simple expression that depends only on $\Delta\mu/\gamma$:

$$\tan\left[\left(1 - 2p_1\right) \frac{\pi}{2}\right] + \tan\left[\left(1 - 2p_0\right) \frac{\pi}{2}\right] = \frac{\Delta\mu}{\gamma}. \quad (5)$$

Example contours are shown in figure 4(b).

⁴Fixed-hypothesis contours on a (p_0, p_1) plot are closely related to ROC (Receiver Operating Characteristic) curves, which have been used for many years in a variety of fields.

⁵Following standard convention we write $T \sim f(t)$ to indicate that f is the pdf of T (use of the ' \sim ' symbol does not imply any kind of approximation).

Example 3: μ is an exponential decay rate:

$$T \sim \mu e^{-\mu t} \quad (6)$$

Here the fixed-hypothesis contours depend only on the ratio of μ_1 to μ_0 :

$$\ln(p_1) = \frac{\mu_1}{\mu_0} \ln(1 - p_0). \quad (7)$$

An interesting generalization is to perform the test on a combination of n independent decay time measurements T_i . In this case the likelihood ratio statistic is a one-to-one function of the sum of the measurements, which we therefore take as our test statistic, $T \equiv \sum_{i=1}^n T_i$. The distribution of T is Gamma(n, μ), with n the shape parameter and μ the rate parameter:

$$T \sim \frac{\mu^n t^{n-1} e^{-\mu t}}{\Gamma(n)}; \quad (8)$$

the fixed-hypothesis contours depend on n and on the ratio μ_1/μ_0 :

$$p_1 = 1 - P\left(n, \frac{1}{2} \frac{\mu_1}{\mu_0} \chi_{2n, p_0}^2\right), \quad (9)$$

where $P(n, z)$ is the regularized incomplete gamma function and $\chi_{2n, p}^2$ is the p -quantile of a chisquared distribution with $2n$ degrees of freedom. Some example contours are shown in figure 4(c). Unlike Gaussian or Cauchy contours, gamma contours are not symmetric around the main diagonal of the plot.

Example 4: μ is a Poisson mean:

$$T \sim \frac{\mu^t}{t!} e^{-\mu} \quad (t \text{ integer}). \quad (10)$$

In this case the contours are discrete and must be computed numerically. Their dependence on μ_0 and μ_1 does not simplify. A few examples are plotted in figure 4(d).

A common feature of examples 1-3 above is that the region of the plot above the diagonal $p_0 + p_1 = 1$ is empty. This is a general consequence of our definition of one-sided p -values, and of the fact, suggested by the requirement $\mu_1 > \mu_0$, that the bulk of the pdf $f_1(t)$ under H_1 lies to the right of the bulk of the pdf $f_0(t)$ under H_0 . In other words, for any t , the area under f_0 and to the right of t is smaller than the corresponding area under f_1 :

$$\text{For all } t : \int_t^\infty f_0(u) du \leq \int_t^\infty f_1(u) du. \quad (11)$$

On the left-hand side one recognizes p_0 and on the right-hand side $1 - p_1$, whence the inequality $p_0 + p_1 \leq 1$ follows. However, this is only strictly true for continuous pdf's. For discrete pdf's, p_0 and p_1 *both* include the finite probability of the observation, so that it may happen that $p_0 + p_1 > 1$ when f_0 and f_1 are very close to each other. This is evident in figure 4(d) for the case $\mu_0 = \mu_1 = 10$.

3.5 Asimov data sets

In a given data analysis problem, any data set (real or artificial) for which the parameter estimators yield the true values is called an Asimov data set [7]. By evaluating a test statistic on an Asimov data set one usually obtains an approximation to the median of that test statistic, and the corresponding p -value will be the median p -value under the assumed hypothesis. Median p -values are used to characterize the sensitivity of an experiment.

A simple example of the use of the fixed-hypothesis contours is that they map the abscissa $p_0 = 0.5$ onto the median value of p_1 under H_0 , and vice-versa, the value $p_1 = 0.5$ is mapped onto the median of p_0 under H_1 . These medians can be directly read off the plot. For the Gaussian case with $\Delta\mu/\sigma = 0.0, 1.67, \text{ or } 3.33$, the median p_1 under H_0 is $0.5, 4.7 \times 10^{-2}, \text{ or } 4.3 \times 10^{-4}$, respectively. By symmetry of the Gaussian density, these values are also those of the median p_0 under H_1 .

By the invariance of probability statements under one-to-one transformations of random variables, the median CL_s under H_0 can be obtained by plugging $p_0 = 1/2$ into the definition of CL_s . This yields:

$$\text{Med}_{H_0}(CL_s) = CL_s|_{p_0=1/2} = \frac{p_1}{1-p_0} \Big|_{p_0=1/2} = 2 p_1|_{p_0=1/2} = 2 \text{Med}_{H_0}(p_1). \quad (12)$$

Assuming H_0 is true, the median CL_s for testing H_1 equals twice the median p_1 .

3.6 Punzi sensitivity

For large enough separation of the pdf's, the fixed-hypothesis contour will keep out of the no-decision region. Punzi [8] defines sensitivity as the expected signal strength required for there to be a probability of at least $1 - \alpha_1$ for claiming a discovery with significance α_0 (e.g. a probability of 95% for discovery at the level of 2.87×10^{-7}). This has the advantage that above the sensitivity limit, the data are guaranteed to provide rejection of H_0 at the significance level α_0 , or exclusion of H_1 at the significance level α_1 , or both; the data cannot fall in the no-decision region. In figure 5, the Punzi sensitivity corresponds to a pdf separation for which the (p_0, p_1) contour (not drawn) passes through the intersection of the vertical dot-dashed and horizontal dashed lines. In the following we refer to this intersection as the 'Punzi point'.

3.7 Effect of one-to-one transformations of the test statistic

P -values are probabilities and therefore remain invariant under one-to-one transformations of the test statistic on which they are based. Plots of p_0 versus p_1 are similarly unaffected, but one must remember that these plots involve two hypotheses, and that effects of a transformation on the pdf's of the test statistic under H_0 and H_1 are different. This is the reason that, for example, the p_0 versus p_1 plot for testing the mode of a Gaussian pdf is not identical to the plot for testing the mode of a Cauchy pdf, even though Gaussian and Cauchy variates are related by one-to-one transformations (see examples 1 and 2 in section 3.4). We take a closer look at this particular case here. Suppose that under H_0 (H_1) the test statistic X is

Gaussian with mean μ_0 (μ_1) and width σ . Then, if H_0 is true, the transformation

$$X \longrightarrow Y \equiv \mu_c + \gamma \tan \left[\frac{\pi}{2} \operatorname{erf} \left(\frac{X - \mu_0}{\sqrt{2} \sigma} \right) \right] \quad (13)$$

maps X into a Cauchy variate Y with mode μ_c and scale parameter γ . If on the other hand H_1 is true, X will be mapped into a variate Y with pdf

$$f(y) = \frac{\exp \left[-\frac{1}{2} \left(\frac{\Delta\mu}{\sigma} \right)^2 + \frac{\sqrt{2}\Delta\mu}{\sigma} \operatorname{erf}^{-1} \left[\frac{2}{\pi} \arctan \left(\frac{y - \mu_c}{\gamma} \right) \right] \right]}{\pi\gamma \left[1 + \left(\frac{y - \mu_c}{\gamma} \right)^2 \right]}, \quad (14)$$

which is an asymmetric density that depends on three parameters: μ_c , γ , and $\Delta\mu/\sigma \equiv |\mu_1 - \mu_0|/\sigma$; it reduces to a Cauchy density in the limit $\Delta\mu/\sigma \rightarrow 0$. Figure 6 compares the two pdf's. Thus, whereas in X space we are testing a Gaussian hypothesis against a Gaussian hypothesis with a different mean, in Y space we are testing a Cauchy hypothesis against a hypothesis with a rather different, asymmetrical distribution. However the p_0 versus p_1 plot is the same in both spaces.

Another interesting property of one-to-one transformations of test statistics is that they preserve the likelihood ratio (since the Jacobian of the transformation cancels in the ratio). Thus, if f_i is the pdf of X under H_i , $i = 0, 1$, and we transform X into Y with pdf's g_i , we have:

$$\frac{g_0(y)}{g_1(y)} = \frac{f_0(x)}{f_1(x)}. \quad (15)$$

Suppose now that the $X \longrightarrow Y$ transformation is the likelihood ratio transformation: $y \equiv f_0(x)/f_1(x)$. Then it follows from the above equation that

$$g_0(y) = y g_1(y), \quad (16)$$

a useful simplification. If one prefers to work with the logarithm of the likelihood ratio, $q \equiv \ln y$, and $h_i(q)$ is the pdf of q under H_i , then one finds:

$$h_0(q) = e^q h_1(q). \quad (17)$$

Suppose for example that $f_i(x)$ is Gaussian with mean μ_i and width σ . The pdf's of the log-likelihood ratio are then:

$$h_0(q) = \frac{1}{\sqrt{2\pi} \Delta\mu/\sigma} \exp \left[-\frac{1}{2} \left(\frac{q - \frac{1}{2} (\Delta\mu/\sigma)^2}{\Delta\mu/\sigma} \right)^2 \right], \quad (18)$$

$$h_1(q) = \frac{1}{\sqrt{2\pi} \Delta\mu/\sigma} \exp \left[-\frac{1}{2} \left(\frac{q + \frac{1}{2} (\Delta\mu/\sigma)^2}{\Delta\mu/\sigma} \right)^2 \right], \quad (19)$$

and it is straightforward to verify equation (17).

The Gauss-versus-Gauss likelihood ratio $f_0(x)/f_1(x)$ in the above example is invariant under translations and rescalings of the original pdf's (i.e. under addition of a common

constant to μ_0 , μ_1 , and x ; and under multiplication of μ_0 , μ_1 , σ , and x by a common factor). These two invariances reduce the three numbers (μ_0 , μ_1 , and σ) required to specify the $f_i(x)$ to a single one ($\Delta\mu/\sigma$) for the $h_i(q)$. Note that $\Delta\mu/\sigma$ is the ratio of the difference in means to the standard deviation for the pair (f_0, f_1) as well as (h_0, h_1) .

More generally, since the likelihood ratio transformation $x \rightarrow q$ is one-to-one, fixed-hypothesis contours obtained from the $h_i(q)$ are identical to those obtained from the $f_i(x)$.

4 Outcome probabilities and error rates

A useful feature of (p_0, p_1) plots is that they help us map probabilities under H_0 to probabilities under H_1 and vice-versa, using a simple graphical method. Suppose for instance that we are interested in the outcome $p_0 \leq 0.3$. When H_0 is true this has probability 0.3, since p_0 is uniformly distributed under H_0 . To find the probability under H_1 we map the interval $0 \leq p_0 \leq 0.3$ onto the p_1 axis using the appropriate contour on figure 5, say the one with $\Delta\mu/\sigma = 1.67$. This yields the interval $0.13 \leq p_1 \leq 1$. Since p_1 is uniform under H_1 , we can conclude that the outcome $p_0 \leq 0.3$ has probability 0.87 under H_1 . In a similar way, it can be read from the figure that rejection of H_0 (the outcome $p_0 \leq \alpha_0$) has probability $1 - \beta_0$ under H_1 , where β_0 is the p_1 coordinate of the intersection of the line $p_0 = \alpha_0$ with the relevant contour. As for rejection of H_1 (the outcome $p_1 \leq \alpha_1$), this has probability $1 - \beta_1$ under H_0 , where β_1 is the p_0 coordinate of the intersection of the line $p_1 = \alpha_1$ with the contour.

The graphical method allows one to derive the probabilities under H_0 and H_1 of the four possible outcomes of the double test (see Table 1). In computing these probabilities

Double Test Outcome	Decision	Probability Under H_0	Probability Under H_1
$p_0 \leq \alpha_0$ & $p_1 \leq \alpha_1$	Reject H_0 Reject H_1	$\max(0, \alpha_0 - \beta_1)$	$\max(0, \alpha_1 - \beta_0)$
$p_0 \leq \alpha_0$ & $p_1 > \alpha_1$	Reject H_0 Fail to reject H_1	$\min(\alpha_0, \beta_1)$	$\min(1 - \alpha_1, 1 - \beta_0)$
$p_0 > \alpha_0$ & $p_1 \leq \alpha_1$	Fail to reject H_0 Reject H_1	$\min(1 - \alpha_0, 1 - \beta_1)$	$\min(\alpha_1, \beta_0)$
$p_0 > \alpha_0$ & $p_1 > \alpha_1$	Fail to reject H_0 Fail to reject H_1	$\max(0, \beta_1 - \alpha_0)$	$\max(0, \beta_0 - \alpha_1)$

Table 1: Possible outcomes of the double-test procedure, together with their probabilities under H_0 and H_1 . As expected, the probabilities under a given hypothesis all add up to one.

one needs to handle separately the cases where the separation between the pdf's under H_0 and H_1 is smaller or larger than that corresponding to the Punzi sensitivity. Consider for example the probability of outcome $p_0 > \alpha_0$ & $p_1 > \alpha_1$ under H_0 . Referring to Figure 5, the contour with $\Delta\mu/\sigma = 3.33$ passes below the Punzi point, so that the desired probability is zero. On the other hand, the contour with $\Delta\mu/\sigma = 1.67$ passes above that point, and

the segment of contour above both the α_0 and α_1 thresholds has probability $\beta_1 - \alpha_0$ under H_0 . The probabilities for these two cases can be summarized as $\max(0, \beta_1 - \alpha_0)$, as shown in the table. An important caveat about the table is that the double test allows for the possibility that an unspecified hypothesis other than H_0 and H_1 could be true, in which case a separate column of probabilities would be needed. It is nevertheless reasonable to use this table for performance optimization purposes, since H_0 and H_1 are the two main hypotheses of interest.

Using Table 1 one can compute various error rates as well as the power of the double test. In analogy with the nomenclature of Neyman-Pearson tests, we can say that there are two Type-I errors, wrong decisions that are made when H_0 is true:

Type-Ia error: Rejecting H_0 when H_0 is true. The probability of this error is

$$\mathbb{P}(p_0 \leq \alpha_0 \mid H_0) = \max(0, \alpha_0 - \beta_1) + \min(\alpha_0, \beta_1) = \alpha_0. \quad (20)$$

This is the Type-I error rate in a standard Neyman-Pearson test of H_0 against H_1 .

Type-Ib error: Failing to reject H_1 when H_0 is true. This has probability

$$\mathbb{P}(p_1 > \alpha_1 \mid H_0) = \min(\alpha_0, \beta_1) + \max(0, \beta_1 - \alpha_0) = \beta_1. \quad (21)$$

It is of course possible to commit both a Type-Ia and a Type-Ib error on the same testing problem. The rate of such double errors is not the product of the individual rates α_0 and β_1 , but rather, as Table 1 indicates, their minimum, $\min(\alpha_0, \beta_1)$. Errors that are made when H_1 is true are called Type II:

Type-IIa error: Rejecting H_1 when H_1 is true. The probability is

$$\mathbb{P}(p_1 \leq \alpha_1 \mid H_1) = \max(0, \alpha_1 - \beta_0) + \min(\alpha_1, \beta_0) = \alpha_1. \quad (22)$$

Type-IIb error: Failing to reject H_0 when H_1 is true. The rate of this error is

$$\mathbb{P}(p_0 > \alpha_0 \mid H_1) = \min(\alpha_1, \beta_0) + \max(0, \beta_0 - \alpha_1) = \beta_0. \quad (23)$$

This is the Type-II error rate in a standard Neyman-Pearson test of H_0 against H_1 .

The rate for committing both Type-II errors simultaneously is $\min(\alpha_1, \beta_0)$. Finally, there is a Type-III error, which has no equivalent in the Neyman-Pearson setup:

Type-III error: Failing to reject H_0 and H_1 when a third, unspecified hypothesis is true. Without additional information about this third hypothesis it is not possible to calculate the Type-III error rate.

Since there is more than one Type-II error, there is some arbitrariness in the definition of the power of the double test. One possibility is to define it as the probability of committing

neither of the two Type-II errors, that is, as the probability of rejecting H_0 *and* failing to reject H_1 , when H_1 is true:

$$\mathbb{P}(p_0 \leq \alpha_0 \ \& \ p_1 > \alpha_1 \mid H_1) = 1 - \min(\alpha_1, \beta_0) = \min(1 - \alpha_1, 1 - \beta_0). \quad (24)$$

This is different from the power of the Neyman-Pearson test, which is $1 - \beta_0$. Equation (24) has a simple interpretation if we look at it in terms of the separation between the H_0 and H_1 pdf's (see figure 1). At low separation, β_0 is large, and the power is dominated by our ability to reject H_0 . At high separation (figure 1c), β_0 is low, and the power is limited by our willingness to accept H_1 (as opposed to a third, unspecified hypothesis).

Instead of using p -values to decide between hypotheses, one can use likelihood ratios to evaluate the evidence against them. In this case error rates are replaced by probabilities of misleading evidence. The corresponding discussion can be found in Section 5.3.

5 Likelihood ratios

Rather than using p -values for discriminating between hypotheses, it is possible to make use of a likelihood ratio⁶; this would also be the starting point for various Bayesian methods.

5.1 Likelihood-ratio contours

It is instructive to plot contours of constant likelihood ratio $\lambda_{01} \equiv L_0/L_1$ on the p_0 versus p_1 plot. This needs some thought however, since a likelihood ratio calculation requires three input numbers (the values μ_0 and μ_1 of the parameter μ under H_0 and H_1 , and the observed value t of the test statistic), whereas a point in the (p_0, p_1) plane only yields two numbers. Our approach here is the following: for a set of contours with given λ_{01} , we fix the null hypothesis μ_0 in order to map p_0 to t , then solve the likelihood-ratio constraint $\lambda_{01} = L_0(t, \mu_0)/L_1(t, \mu_1)$ for μ_1 , and finally use t and μ_1 to obtain p_1 . In this way, both the likelihood ratio and the value of μ under H_0 are constant along our likelihood-ratio contours, but in general the value of μ under H_1 varies point by point.

If the test statistic t itself is the likelihood ratio, the above procedure needs to be adjusted, since now the pdf's of t under H_0 and H_1 depend on both μ_0 and μ_1 (see for example equations (18) and (19) in section 3.7). There is no longer a likelihood-ratio constraint to solve. Instead, for pre-specified values of μ_0 and $t \equiv \lambda_{01}$, one maps p_0 into μ_1 , and substitutes t , μ_0 and μ_1 into the expression for p_1 .

Remarkably, for some of the simple cases examined in section 3.4 it turns out that the likelihood-ratio contours are independent of μ_0 and μ_1 . The contours do depend on the family of pdf's to which the data are believed to belong, but not on the particular family members specified by the hypotheses. For the examples of section 3.4, the likelihood-ratio contours take the following forms:

Example 1: μ is the mean of a Gaussian distribution of known width σ :

$$\left[\operatorname{erf}^{-1}(1 - 2p_1) \right]^2 - \left[\operatorname{erf}^{-1}(1 - 2p_0) \right]^2 = \ln(\lambda_{01}). \quad (25)$$

⁶Note that a likelihood ratio can be used as a test statistic T within a p -value method, or directly, without the calibration provided by p -values. It is the latter case that we are considering in this section.

Example 2: μ is the mode of a Cauchy distribution with known half-width at half-height γ :

$$\frac{1 + \left[\tan\left(\left(1 - 2p_1\right)\frac{\pi}{2}\right) \right]^2}{1 + \left[\tan\left(\left(1 - 2p_0\right)\frac{\pi}{2}\right) \right]^2} = \lambda_{01}. \quad (26)$$

Example 3: μ is an exponential decay rate:

$$\left[\frac{P^{-1}(n, p_0)}{P^{-1}(n, 1 - p_1)} \right]^n e^{P^{-1}(n, 1 - p_1) - P^{-1}(n, p_0)} = \lambda_{01}, \quad (27)$$

where $P^{-1}(n, x)$ is the inverse, with respect to the second argument, of the regularized incomplete gamma function (i.e., $y = P^{-1}(n, x)$ is equivalent to $x = P(n, y)$).

Example 4: μ is a Poisson mean:

There is no closed analytical expression, and the contours, which must be computed numerically, depend on μ_0 and μ_1 (as opposed to just their difference or their ratio).

Figure 7 shows the $\lambda_{01} = 0.37, 0.83, 1.0, 1.2$ and 2.7 contours for these four cases. Along the diagonal $p_1 = 1 - p_0$ (or close to it in the Poisson case), the H_0 and H_1 pdf's are identical and λ_{01} is unity. For symmetric pdf's such as the Gaussian and Cauchy, the likelihood ratio is also unity along the other diagonal line, $p_1 = p_0$. This is because the observed value of the test statistic is then situated midway between the pdf peaks. For asymmetric pdf's such as the gamma and Poisson the likelihood ratio is no longer unity when $p_1 = p_0$, but there is still a $\lambda_{01} = 1$ contour that starts at the origin of the plot and rises toward its middle. Above and to the left of this curve, the likelihood ratio favors H_1 ; below it, H_0 is favored.

Loosely stated, the central limit theorem asserts that the distribution of the mean of n measurements converges to a Gaussian as the sample size n increases. When the test statistic is defined as such a mean, likelihood ratio contours will converge to their shape for a Gauss versus Gauss test. This is illustrated in figure 8 for the exponential/gamma case and in figure 9 for the Poisson case.

5.2 Comparison of p-values and likelihood ratios

A criticism against p -values is that they overstate the evidence against the null hypothesis [9, 10]. One aspect of this is that p -values tend to be impressively smaller than likelihood ratios. The fact that they are not identical is no surprise. Likelihoods are calculated as the height of the relevant pdf at the observed value of the statistic T , while p -values use the corresponding tail area. Furthermore a p -value uses the pdf of a single hypothesis, while a likelihood ratio requires the pdf's of two hypotheses. As can be seen from figure 10, at constant p_0 (even if it is very small) L_0/L_1 can have a range of values, sometimes favoring H_1 , sometimes H_0 . This will depend on the separation of the pdf peaks. Thus for Gaussian pdf's, a p_0 value of 3×10^{-7} will favor H_1 provided $0 < \Delta\mu/\sigma < 10$, but for larger $\Delta\mu/\sigma$ the observed test statistic is closer to the H_0 peak than to H_1 's, and so even though the data are very inconsistent with H_0 , the likelihood ratio still favors H_0 as compared with H_1 .

Another example is given in Table 2; this uses simple Poisson hypotheses for both H_0 and H_1 . It involves a counting experiment where the null hypothesis H_0 predicts 1.0 event

	First data set	Second data set
H_0	Poisson, $\mu = 1$	Poisson, $\mu = 10$
H_1	Poisson, $\mu = 10$	Poisson, $\mu = 100$
n_{obs}	10	30
p_0	1.1×10^{-7} 5.2σ	2.5×10^{-7} 5.0σ
p_1	0.58 -0.2σ	2.2×10^{-16} 8.1σ
L_0/L_1	8×10^{-7} Strongly favors H_1	$1.2 \times 10^{+9}$ Strongly favors H_0

Table 2: Comparing p -values and likelihood ratios

and the alternative H_1 predicts 10.0 events. In a first run 10 events are observed; both p_0 and the likelihood ratio disfavor H_0 . Then the running time is increased by a factor of 10, so that the expected numbers according to H_0 and H_1 both increase by a factor of 10, to 10.0 and 100.0 respectively. With 30 observed events, p_0 corresponds to about 5σ as in the first run, but despite this the likelihood ratio now strongly favors H_0 . This is simply because the 5σ $n_{obs} = 10$ in the first run was exactly the expected value for H_1 , but with much more data the 5σ $n_{obs} = 30$ is way below the H_1 expectation. In fact, in the second run, the p -value approach rejects both H_0 and H_1 .

More data corresponds to increasing pdf separation. Thus we are moving downwards on a line at constant p_0 , resulting in a smaller p_1 , and provided $p_1 < 1/2$, a larger L_0/L_1 . This is one motivation for hypothesis selection criteria that employ a decreasing value for the rejection threshold α_0 as the amount of data increases.

It is interesting to contrast the exclusion regions for H_1 provided by cuts on p_1 and on the likelihood ratio $L_0/L_1 = \lambda_{01}$ (see figures 2 and 7 respectively). The main differences are at small and at large p_0 , where the excluded region extends up to $p_1 = \alpha_1$ for p_1 cuts, but to much smaller p_1 values for cuts on the likelihood ratio. At large p_0 , the likelihood cuts resemble more those provided by CL_s (see figure 2). At small p_0 , the likelihood cuts correspond to the exclusion p_1 cut-off α_1 effectively decreasing as the H_0 and H_1 pdf's become more separated (e.g., as the amount of data collected increases).

5.3 Probability of misleading evidence in likelihood ratio tests

When studying the evidence provided by the likelihood ratio L_0/L_1 in favor of hypothesis H_0 , an important quantity is the probability of misleading evidence. This is defined by Royall [11] as the probability of observing $L_0/L_1 > k$, for a given $k > 1$, when H_1 is true. Figure 10 shows how this probability can be determined by drawing the appropriate fixed-hypothesis contour (dashed line, here corresponding to $\Delta\mu/\sigma = 1.67$) on top of the likelihood-ratio contour of interest (here $L_0/L_1 = 1.2$). Larger likelihood-ratio contours intersect the dashed line at lower values of p_1 . Therefore the probability of a larger likelihood ratio under H_1 ,

i.e., the probability of misleading evidence, is given by the p_1 -coordinate of the intersection point X.

It is of course also possible to calculate the probability of misleading evidence that favors H_1 when H_0 is actually true. For this we look at the intersection of a fixed-hypothesis contour with a likelihood-ratio contour for which $L_0/L_1 < 1$, and we are concerned about even smaller likelihood ratio values⁷. The probability of misleading evidence is then given by the p_0 -coordinate of that intersection.

Careful inspection of the shape of the likelihood-ratio contours in figure 10 reveals that the probabilities of misleading evidence are small at small values of $\Delta\mu/\sigma$ (where there is little chance of obtaining strong evidence in favor of either hypothesis), then increase to a maximum, and finally become small again at large $\Delta\mu/\sigma$.

The determination of probabilities of misleading evidence from p_0 and p_1 coordinates may give the impression that these probabilities could be calculated from the observed likelihood ratio and reported ‘post-data’. According to the likelihoodist paradigm of statistics, this view is incorrect. As emphasized in ref. [11], *all* the relevant evidence about the hypotheses is contained in the likelihood ratio. The probabilities of misleading evidence should only be used for experiment-planning purposes, by calculating them for standard likelihood ratio values. By convention, a value of $L_0/L_1 = 8$ is defined as ‘fairly strong’ evidence in favor of H_0 , whereas $L_0/L_1 = 32$ is said to be ‘strong’ evidence. Likelihood-ratio contours for these values would not be visible on a linear plot such as figure 10. As shown in figure 11, a log-log plot gives much better visualization.

6 Famous puzzles in statistics

The topic of p -values has generated many controversies in the statistics literature. In this section we use p_0 versus p_1 plots to discuss a couple of famous puzzles that initiated some of these controversies.

6.1 Sampling to a foregone conclusion

Suppose that in searching for a new physics phenomenon we adopt the following procedure:

1. Choose a discovery threshold α_0 , and let \mathcal{E} be a set of candidate events, initially empty.
2. Add one candidate event to \mathcal{E} and compute p_0 , the p -value to test the background-only hypothesis H_0 based on all events in \mathcal{E} .
3. If $p_0 \leq \alpha_0$, reject H_0 , claim discovery, and stop; otherwise go back to step 2.

If the new physics phenomenon can be modeled by a simple hypothesis H_1 , we can also compute the p -value p_1 at step 2, and the whole procedure can be represented by a random walk in the p_0 versus p_1 plane. At each step of the walk, the p -values are updated with the

⁷Just as the cut-offs α_0 and α_1 for p_0 and p_1 are usually taken to be (very) different, similarly when using likelihood ratio cuts there is generally no necessity for one to be the reciprocal of the other.

addition of a random new event. Four examples of such random walks are shown in figure 12, two assuming that H_0 is true, and two assuming that H_1 is true.

What is the chance of the above procedure stopping *when H_0 is true*? In other words, what is the probability of incorrectly claiming discovery with this procedure? The answer, perhaps surprisingly, is 100%, due to a result from probability theory known as the Law of the Iterated Logarithm (LIL). The latter applies to any sequence of random variables $\{X_1, X_2, X_3, \dots\}$ that are independent and identically distributed with finite mean μ_0 and variance σ^2 . Consider the Z -values constructed from partial sums of the X_i :

$$Z_n = \frac{\frac{1}{n} \sum_{i=1}^n X_i - \mu_0}{\sigma/\sqrt{n}}, \quad \text{for } n = 1, 2, 3, \dots \quad (28)$$

The LIL states that with probability 100% the inequality

$$|Z_n| \geq (1 + \delta) \sqrt{2 \ln \ln n} \quad (29)$$

holds for only finitely many values of n when $\delta > 0$ and for infinitely many values of n when $\delta < 0$. At large n the Z_n will be approximately standard normal and correspond to the p -values

$$p_0(n) = \int_{|Z_n|}^{\infty} \frac{e^{-t^2/2}}{\sqrt{2\pi}} dt = \frac{1}{2} \left[1 - \operatorname{erf} \left(\frac{|Z_n|}{\sqrt{2}} \right) \right], \quad (30)$$

so that the LIL of eqn. 29 can be rephrased as stating that, as n increases, the inequality

$$p_0(n) \leq \frac{1}{2} \left[1 - \operatorname{erf} \left((1 + \delta) \sqrt{\ln \ln n} \right) \right] \quad (31)$$

occurs infinitely many times if $\delta < 0$. In particular, regardless of how small α_0 is, at large n the right-hand side of (31) will become even smaller; therefore, if $\delta < 0$ the LIL *guarantees* that $p_0(n)$ will cross the discovery threshold at some n , allowing the search procedure to stop with a discovery claim. Crucial to this guarantee is the fact that inequality (31) occurs *infinitely* many times for $\delta < 0$; it will then *certainly* occur at n large enough to force a crossing of the discovery threshold. In contrast, for $\delta > 0$ there is a value of n beyond which there are no crossings (and there may indeed be none at all for any n); rejection of H_0 is not guaranteed to occur.

In terms of designing a coherent search procedure, one can view the LIL as defining an n -dependent boundary

$$\alpha_{\text{LIL}}(n) = \frac{1}{2} \left[1 - \operatorname{erf} \left(\sqrt{\ln \ln n} \right) \right]. \quad (32)$$

Any discovery threshold with an n -dependence that causes it to exceed this boundary at large n is unsatisfactory since it is guaranteed to be crossed. It is instructive to draw the LIL boundary on a p_0 versus p_1 plot. To each value of n there corresponds a fixed-hypothesis contour on the plot (see figure 13). When testing H_0 , one point on the LIL boundary is then given by the intersection of that contour with the line $p_0 = \alpha_{\text{LIL}}(n)$. By connecting all such points across contours one obtains the blue lines drawn in figure 13 and in figure 12(a) and (c) (note that $n = 2$ is the smallest integer for which $\alpha_{\text{LIL}}(n)$ can be computed). When testing H_1 , the LIL boundary is given by the intersections of the contours with the lines $p_1 = \alpha_{\text{LIL}}(n)$, as shown in figure 12(b) and (d).

Focusing on plots (a) and (c) of figure 12, we note that when H_0 is true, the p_1 coordinate of random walks tends to decrease very rapidly as a function of n . The p_0 coordinate is more stable, but it does exhibit occasional excursions towards low p_0 values. The LIL states that the number of such excursions to the left of the blue line is finite (not infinite) as n goes to infinity. However, any threshold curve to the right of the blue line will be crossed infinitely many times. A constant threshold of the form $p_0 = \alpha_0$ will be to the right of the blue line at large n and is therefore unsatisfactory, in contrast with a threshold curve in the form of a likelihood ratio contour (see figure 12) or with an n dependence of the form α_0/\sqrt{n} (see figure 13).

In particle physics we have constant thresholds of 3σ ($\alpha_0 = 1.35 \times 10^{-3}$) and 5σ ($\alpha_0 = 2.87 \times 10^{-7}$). Due to the iteration of logarithms in the LIL, it takes an enormously large value of n for the blue line to cross these thresholds, so that the problem is not practically relevant. The statistician I. J. Good once remarked that a statistician could “cheat by claiming at a suitable point in a sequential experiment that he has a train to catch [...] But note that the iterated logarithm increases with fabulous slowness, so that this particular objection to the use of tail-area probabilities is theoretical rather than practical. To be reasonably sure of getting 3σ one would need to go sampling for billions of years, by which time there might not be any trains to catch.” [12]

The LIL provides the weakest known constraint on the n -dependence of discovery thresholds. It is a purely probabilistic characterization of tail probabilities under a single hypothesis. Much more stringent constraints can be obtained by introducing an alternative hypothesis and using statistical arguments (see for example [13]).

6.2 The Jeffreys-Lindley paradox

The Jeffreys-Lindley paradox occurs in tests of a simple H_0 versus a composite H_1 , for example:

$$H_0 : \mu = \mu_0 \quad \text{versus} \quad H_1 : \mu > \mu_0. \quad (33)$$

The paradox is that for some values of the observed test statistic t , the value of p_0 can be small enough to cause rejection of H_0 while the Bayes factor favors H_0 . Writing L_0 , $L_1(\mu)$ for the likelihood under H_0 , respectively H_1 , the Bayes factor is defined by

$$B_{01} \equiv \frac{L_0}{\int L_1(\mu) \pi_1(\mu) d\mu}, \quad (34)$$

where $\pi_1(\mu)$ is a prior density for μ under H_1 . In order to understand the origin of the paradox, it helps to note that this Bayes factor can be rewritten as a weighted harmonic average of likelihood ratios:

$$B_{01} = \left[\int \frac{1}{\lambda_{01}(\mu)} \pi_1(\mu) d\mu \right]^{-1}, \quad (35)$$

with $\lambda_{01}(\mu) \equiv L_0/L_1(\mu)$. As this formula suggests, it will prove advantageous to look at the composite H_1 as a collection of simple hypotheses about the value of μ , each with its own simple-to-simple likelihood ratio $\lambda_{01}(\mu)$ to the null hypothesis H_0 .

In the following subsection we use this idea to develop basic insight into the origin of the Jeffreys-Lindley paradox. Later subsections take a deeper look at the conditions under which the paradox appears and at possible solutions.

6.2.1 Basic insight

Figure 14 illustrates the paradox for the case where the pdf of the test statistic t is Gaussian with mean μ and standard deviation $\sigma = 1$. As in Section 5.2, consider a vertical line at the relevant p_0 in plot (a); this crosses a series of different λ_{01} contours. At point b , the H_0 and H_1 pdf's are identical (see plot (b)), and the likelihood ratio is unity. Point c is at $p_1 = 0.5$, with the H_1 pdf having its maximum exactly at the position of the data statistic t . The likelihood ratio now favors H_1 , and is in agreement with the small p_0 value in rejecting H_0 . Plots (d) and (e) show even larger separations between H_0 and H_1 . In plot (d), corresponding to point d in plot (a), the position of the H_1 pdf is such that the data statistic t is midway between the H_0 and H_1 peaks. Thus $p_0 = p_1$ and point d lies on the diagonal of plot (a), with the likelihood ratio again unity. Finally, with the larger separation of plot (e), the likelihood ratio now favors H_0 , even though p_0 is small; the likelihood ratio and p_0 lead to opposite conclusions.

To go from the series of simple H_1 's to the composite H_1 with unspecified μ in the Jeffreys-Lindley paradox, we take the weighted harmonic average of the likelihood ratios λ_{01} , with the weighting given by the prior $\pi_1(\mu)$ as in equation (35). As we integrate along the vertical line in plot (a), the contributions between points b and d favor H_1 . Lower down, from d to e and beyond, H_0 is favored. The Bayes factor will thus end up favoring H_0 if the integration range is wide enough⁸ and suitably weighted by the prior $\pi_1(\mu)$. This explains the mechanism by which the Jeffreys-Lindley paradox can occur.

6.2.2 Regions in the plane of p_0 versus prior-predictive p_1

To visualize the conditions under which the Jeffreys-Lindley paradox appears, we generalize the p_0 versus p_1 plot to the case of a composite H_1 by making use of the prior-predictive p -value [14]; this is a prior-weighted average p -value over H_1 :

$$p_{1pp} \equiv \int \pi_1(\mu) \int_{-\infty}^{t_0} f(t | \mu) dt d\mu, \quad (36)$$

where $f(t | \mu)$ is the pdf of T and t_0 its observed value. To fix ideas, assume that f is Gaussian with mean μ and standard deviation σ (not necessarily equal to 1), and that the prior $\pi_1(\mu)$ is the indicator function of the interval $[\mu_0, \mu_0 + \tau]$ for some positive τ :

$$\pi_1(\mu) \equiv \pi_1(\mu | \tau) = \frac{1}{\tau} \mathbb{1}_{[\mu_0, \mu_0 + \tau]}(\mu) = \begin{cases} \frac{1}{\tau} & \text{if } \mu_0 < \mu \leq \mu_0 + \tau, \\ 0 & \text{otherwise.} \end{cases} \quad (37)$$

⁸The value of μ , which determines the separation between the corresponding simple H_1 and H_0 , varies non-linearly with distance along the line $bcde$, such that there is generally a far wider range of μ values below the diagonal than above it.

In the absence of detailed prior information about μ , one could think of this prior as modeling the range of μ values deemed to be theoretically and/or experimentally relevant for the search experiment of interest. In any case the exact shape of π_1 is not material to the paradox, only the ratio of length scales τ/σ is. Reference [15] discusses the choice of τ in several particle physics experiments.

Use of p_{1pp} calls for a couple of caveats. First, a small value of p_{1pp} does not imply that all values of μ under H_1 are disfavored. In general it only provides evidence against the overall model (prior plus pdf) under H_1 . However with the particular choice of prior (37), and assuming that τ/σ is sufficiently large, small p_{1pp} implies that the vast majority of μ values under H_1 are unable to explain the data. Second, the distribution of p_{1pp} under a fixed value of μ in H_1 is not uniform. Hence, in a linear plot of p_0 versus p_{1pp} , distances along the p_{1pp} axis cannot be interpreted as probabilities under a fixed μ in H_1 (contrast Section 4). However, such distances can still be interpreted as prior-predictive probabilities, with pdf given by the integral of $f(t | \mu)$ over $\pi_1(\mu)$.

Figure 15 shows fixed-hypothesis contours (fixed μ_0 , σ , and τ) and constant Bayes factor contours in the p_0 versus p_{1pp} plane. For the testing situation examined here, fixed-hypothesis contours only depend on the ratio τ/σ and are labeled accordingly. The constant Bayes factor contours are labeled by the value of B_{01} . For $\tau/\sigma = 0$, H_1 coincides with H_0 and the resulting fixed-hypothesis contour is a subset of the $B_{01} = 1$ contour. As τ/σ increases, the ability of the test to distinguish between H_0 and H_1 also increases. Figure 16 presents a log-log version of the same plot. This allows the drawing of contours with a wider range of Bayes factor values, $B_{01} = 1, 3, 20, \text{ and } 150$. According to ref. [16], a Bayes factor between 1 and 3 represents evidence “not worth more than a bare mention;” between 3 and 20, “positive;” between 20 and 150, “strong;” and greater than 150, “very strong.” One can identify the following regions in the plot:

Upper Left: At small values of p_0 and small values of τ/σ (red contour region), the Bayes factors disfavor H_0 . There is agreement between Bayes factors and p -values.

Lower Left: At small values of p_0 and large values of τ/σ (green contour region), the Bayes factors favor H_0 . There is disagreement between Bayes factors and p -values. This is where the Jeffreys-Lindley paradox shows up. For a numerical example, consider a p_0 value of 2.87×10^{-7} (5σ); the corresponding Bayes factor in favor of H_0 will then be 1, 3, 20, or 150, if the ratio τ/σ is approximately 6.7×10^5 , 2.0×10^6 , 1.3×10^7 , or 1.0×10^8 , respectively. Note the extremely large values of τ/σ required for producing the paradox. This is a consequence of the stringent 5σ convention applied to discovery claims in particle physics.

Upper Right: This is a region with relatively large values of p_0 and p_1 , and where the Bayes factor hovers around 1. Regardless of how one looks at it, there is not enough evidence to decide between H_0 and H_1 .

Lower Right: Here p_1 is small and B_{01} large. Both support the rejection of H_1 in favor of H_0 .

Curves of constant τ/σ represent fixed experimental conditions, such that repeated observations would fall randomly (but not necessarily uniformly) along one such curve. On a

given curve there is agreement between p -values and Bayes factors at high and low p_0 , but somewhere in between there is a region of either no-decision (low τ/σ) or paradox (high τ/σ).

6.2.3 Possible solutions to the paradox

Over the years many solutions have been proposed to the Jeffreys-Lindley paradox. Here we briefly illustrate two arguments.

The first argument essentially blames the p -value method for the paradox and argues that with increasing values of τ/σ the p -value discovery threshold α_0 should be lowered. This argument is usually applied to the situation where σ depends on a sample size n , so that τ/σ is proportional to \sqrt{n} . In figure 16 for example, one could think of the contours $\tau/\sigma = 1, 10, 100, \dots$ as corresponding to $n = 1, 100, 10000, \dots$, respectively. If one chooses a discovery threshold of 1% on the $\tau/\sigma = 1$ contour, 0.1% on the $\tau/\sigma = 10$ contour, and so on, the dot-dashed curve labeled $p_0 = \alpha_0/\sqrt{n}$ (where α_0 is the discovery threshold on the $\tau/\sigma = 1$ contour) is obtained. At large τ/σ this curve follows pretty closely the shape of the constant Bayes factor contours. Thus, cutting on $p_0 < \alpha_0/\sqrt{n}$ instead of $p_0 < \alpha_0$ avoids the Jeffreys-Lindley paradox. Interestingly, this is the same solution that was proposed to avoid sampling to a foregone conclusion in section 6.1.

In a similar vein, it has been argued [17] that for experiments that collect more and more data, the realistic values of μ to be considered under H_1 (assuming that no evidence for $\mu > \mu_0$ has been obtained, and we still believe that a small difference is possible) should be those that are closer and closer to μ_0 . Thus the prior $\pi_1(\mu | \tau)$ in equation (37) should become narrower (smaller τ), and this prevents B_{01} favoring H_0 (as shown in figure 16).

For the second argument, note that in the region of disagreement between p_0 and Bayes factors, both p_0 and p_{1pp} tend to be small: one is in the double-rejection region of the test for most values of μ under H_1 . This should alert the experimenter to the possibility that a third hypothesis may be true, or that there may be a mismodeling error. One such error could be that H_0 , rather than a point null hypothesis, is in fact an interval hypothesis with width ϵ . Thus, instead of (33), one should really be testing

$$H_0 : \mu_0 - \epsilon < \mu \leq \mu_0 \quad \text{versus} \quad H_1 : \mu > \mu_0. \quad (38)$$

We consider two different regimes for ϵ . The first has $\epsilon/\sigma = 0.01$ or 1, corresponding to a small or moderate widening of the original H_0 . The second regime uses $\epsilon/\sigma = 100$ or 10^4 , which almost changes H_0 to $\mu \leq \mu_0$, the complement of $H_1 : \mu > \mu_0$. For both regimes one will need to introduce a prior $\pi_0(\mu)$ for μ under H_0 , and the Bayes factor becomes:

$$B_{01} \equiv \frac{\int L_0(\mu) \pi_0(\mu) d\mu}{\int L_1(\mu) \pi_1(\mu) d\mu}. \quad (39)$$

For the p -value under H_0 one could again consider a prior-predictive version:

$$p_{0pp} \equiv \int \pi_0(\mu) \int_{t_0}^{+\infty} f(t | \mu) dt d\mu, \quad (40)$$

or choose a frequentist approach, such as the supremum p -value [18]:

$$p_{0\text{ sup}} \equiv \sup_{\mu \in [\mu_0 - \epsilon, \mu_0]} \int_{t_0}^{+\infty} f(t | \mu) dt. \quad (41)$$

Figures 17 and 18 illustrate the effect of these two definitions on the Jeffreys-Lindley paradox. Note first that in both cases one recovers figure 16 when ϵ/σ is small. When the prior-predictive p_{0pp} of equation (40) is used (figure 17), a given observation above μ_0 becomes more significant since its p_0 -value is averaged over μ values below μ_0 . This causes the fixed-hypothesis contours to be compressed towards low p_0 . At the same time, the Bayes factor of such an observation tends to decrease due to the numerator being replaced by an average; this causes the constant Bayes factor contours to move down. The net effect of these contour changes is to leave the paradox in place. This can be seen, for example, by considering the point with $p_0 = 10^{-4}$ on the $\tau/\sigma = 10\,000$ contour. In all four plots of figure 17 this point hardly moves, having a Bayes factor B_{01} close to 3.

On the other hand, when the supremum p -value of equation (41) is used for p_0 (figure 18), only the constant Bayes factor contours change. The fixed-hypothesis contours stay the same, because the supremum of p_0 over the interval $[\mu_0 - \epsilon, \mu_0]$ is attained at $\mu = \mu_0$ ⁹. For fixed τ/σ , increasing ϵ/σ causes the paradoxical region to be pushed toward larger values of p_0 and smaller values of p_1 . Eventually the p -values agree with the Bayes factor and the paradox disappears. In principle one could even tune the value of ϵ/σ to obtain $B_{01} = 1$ at a specified value of p_0 (keeping τ/σ constant). Smaller values of p_0 would then correspond to B_{01} disfavoring H_0 , and larger p_0 to B_{01} favoring H_0 .

We conclude from this discussion of the second argument that introduction of a scale ϵ under H_0 is by itself not sufficient to suppress the paradox. One also needs to specify how to handle ϵ in the computation of p_0 . Furthermore, as shown in figure 18 the paradox is not fully suppressed unless ϵ/σ is substantially larger than 1, of the same order as τ/σ . Thus, the hierarchy $\epsilon \ll \sigma \ll \tau$, presented in ref. [15], is sufficient to produce the paradox, but not necessary. When using the supremum p -value, the condition [$\epsilon \ll \tau$ and $\sigma \ll \tau$] is both necessary and sufficient.

6.2.4 Simple versus simple version of the Jeffreys-Lindley paradox

Figures 15 and 16 do not look very different from figures 10 and 11 discussed in the sections on likelihood ratios, in spite of the use of a different p_1 definition. This is a consequence of the fact that the Jeffreys-Lindley paradox can be reformulated in the context of a simple versus simple test¹⁰. As noted at the beginning of section 6.2, the paradox occurs for tests of the form:

$$\text{Test 1: } H_0 : \mu = \mu_0 \text{ versus } H_1 : \mu > \mu_0, \quad (42)$$

using a test statistic $T \sim f(t | \mu)$ and assuming a prior $\pi_1(\mu | \tau)$ for μ under H_1 , where τ characterizes the scale of π_1 .

⁹Note that the supremum of p_1 over the interval $[\mu_0, \mu_0 + \tau]$ is also attained at $\mu = \mu_0$, so that $p_{0\text{ sup}} + p_{1\text{ sup}} = 1$ (for continuous pdf's). Therefore there is nothing to be learned from a plot of $p_{0\text{ sup}}$ versus $p_{1\text{ sup}}$.

¹⁰The simple versus simple scenario outlined in this section is unrelated to the basic insight described in section 6.2.1.

To proceed with the reformulation, introduce a variate X whose randomness is the result of a two-step generating process: $X \sim f(x | \mu)$, where $\mu \sim \pi_1(\mu | \theta)$. Thus, for fixed θ the distribution of X is:

$$\tilde{f}(x | \theta) = \int \pi_1(\mu | \theta) f(x | \mu) d\mu. \quad (43)$$

If for example $f(x | \mu)$ is Gaussian with mean μ and standard deviation σ , and $\pi_1(\mu | \theta)$ is the indicator function of the interval $[\mu_0, \mu_0 + \theta]$, this will yield:

$$\tilde{f}(x | \theta) = \frac{1}{2\theta} \left[\operatorname{erf} \left(\frac{\mu_0 + \theta - x}{\sqrt{2}\sigma} \right) - \operatorname{erf} \left(\frac{\mu_0 - x}{\sqrt{2}\sigma} \right) \right]. \quad (44)$$

As $\theta \rightarrow 0$ this pdf approaches $f(x | \mu_0)$, and we will assume that this remains true for any choice of prior π_1 (i.e., that for $\theta = 0$, $\pi_1(\mu | \theta)$ is a delta function at $\mu = \mu_0$).

Consider now the simple versus simple test:

$$\text{Test 2: } H_0 : \theta = 0 \text{ versus } H_1 : \theta = \tau, \quad (45)$$

using the test statistic $X \sim \tilde{f}(x | \theta)$. Test 2 is designed to determine whether or not the additional source of randomization π_1 is present in the process that generates X . If $\theta = 0$, there is no additional randomization and $\mu = \mu_0$. On the other hand, if $\theta = \tau$, additional randomization is present, its magnitude agrees with the prediction under H_1 in Test 1, and we must have $\mu > \mu_0$. Tests 1 and 2 yield the same information about μ . However, since H_1 is composite in Test 1 but simple in Test 2, this has some interesting consequences. The p -value p_1 is prior-predictive in Test 1 but standard frequentist in Test 2 (as can be seen by interchanging the order of integration in equation (36)). The Bayes factor in Test 1 is a likelihood ratio for Test 2. Tests 1 and 2 yield the same p_0 versus p_1 plots. The Jeffreys-Lindley paradox, which is a disagreement between p -values and Bayes factors in Test 1, is a disagreement between p -values and likelihood ratios in Test 2. This purely frequentist version of the Jeffreys-Lindley paradox is illustrated in figure 19 using the pdf $\tilde{f}(x | \theta)$ of equation (44). It shows that when testing a narrow distribution against a very broad one, it is possible to observe data with small p -value under the narrow-distribution hypothesis and yet large likelihood ratio in favor of that hypothesis.

Even though Test 1 is not of the simple versus simple type, it is possible to define a likelihood ratio statistic for it, as the ratio of the likelihood under H_0 to the maximized likelihood under H_1 , where the maximum is taken over $\mu > \mu_0$. An interesting quantity is the Ockham factor, defined as the ratio of the Bayes factor to this likelihood ratio. For Test 1 the Ockham factor is approximately $\tau/(\sqrt{2\pi}\sigma)$. This is approximately proportional to the ratio of the widths of the distributions under H_1 and H_0 in Test 2. More interestingly, at large τ/σ the Type-II error rate of the simple versus simple test equals $N_\sigma\sigma/\tau$, where N_σ is the number of standard deviations corresponding to the cutoff α_0 used to reject H_0 . Hence the Type-II error rate is inversely proportional to the Ockham factor: if the alternative hypothesis is true, the probability of rejecting the null with p_0 increases with τ/σ , but so does the disagreement between p_0 and B_{01} ! Referring again to figure 19, we see that for small x values (say below $x = 2$), Bayes factors and p -values both favor H_0 . At high x they both disfavor H_0 . In between there is a region where agreement between p -values and Bayes factors depends on the Ockham factor.

7 Nuisance parameters

There are many methods for eliminating nuisance parameters from p -value calculations (see for example [18]), and the choice of method will generally have an effect on the construction of p_0 versus p_1 plots. We start with a couple of examples.

First consider the situation where one makes n measurements x_i from a Gaussian population with unknown mean μ and unknown width σ . A sufficient statistic consists of the pair (\bar{x}, s) , where $\bar{x} = \frac{1}{n} \sum_{i=1}^n x_i$ is the sample mean and $s = [\frac{1}{n-1} \sum_{i=1}^n (x_i - \bar{x})^2]^{1/2}$ is the sample standard deviation. To test the hypotheses $H_i : \mu = \mu_i$ ($i = 0, 1$), the classical approach uses the test statistics $t_i = \sqrt{n}(\bar{x} - \mu_i)/s$, which have Student's t distribution under the respective H_i . Thus one can calculate the p -values p_0 and p_1 . Unfortunately the relation between p_0 and p_1 is not one-to-one: from p_0 one can obtain t_0 , but from t_0 one cannot extract both \bar{x} and s , which are needed to compute t_1 and then p_1 . Hence it is not possible to make a plot of p_0 versus p_1 . This problem is related to the fact that the power of the t test depends on the unknown value of σ and not just on the significance threshold α .

For the second example we consider the observation of a Poisson variate N , whose mean is the product of a parameter of interest μ and a nuisance parameter κ . Again we wish to test $H_0 : \mu = \mu_0$ versus $H_1 : \mu = \mu_1$. Information about the nuisance parameter comes from a second Poisson measurement K , with mean κ . A well-known approach for this case is to condition on the sum $N + K$. The distribution of N , given a fixed value of $N + K$, is binomial with parameter $\mu/(1 + \mu)$. Here one can calculate conditional p -values p_0 and p_1 , and plot one against the other.

The above examples rely on a special structure of the problem under study to eliminate nuisance parameters. Unfortunately such a special structure is not always available, and even when it is, it does not guarantee that a (p_0, p_1) plot can be constructed. Here we offer a couple of suggestions for handling the general case. The first one is to use parametric bootstrap techniques to eliminate the nuisance parameters. To first order these techniques consist in substituting an estimate for the unknown nuisance parameter values. The resulting p -values are generally no longer uniform under their respective null hypothesis, but there exist higher-order refinements that restore some of that uniformity [19]. Bootstrap computations can quickly become rather intensive, but they have the advantage of being frequentist and therefore preserving the error structure of the tests discussed in section 4. As for the likelihood ratios, they can be replaced by profile likelihood ratios. Although the latter are not genuine likelihood ratios, with some caveats they can still be treated as representing statistical evidence in large samples [11].

Our second suggestion is to apply Bayesian methods on the nuisance parameters. Effectively, this amounts to replacing composite hypotheses by simple ones, by integrating out the nuisance parameters over an appropriate proper prior. Suppose for example that the probability density of the data x under H_i is given by $f(x | \mu_i, \nu)$, with ν a vector of nuisance parameters with prior $\pi(\nu)$. Then we simply replace f by

$$f^*(x | \mu_i) = \int f(x | \mu_i, \nu) \pi(\nu) d\nu \quad (46)$$

in the formulation of the hypotheses. The p -values become *prior-predictive* p -values:

$$\begin{aligned} p_i^* &= \int_{x_0}^{\infty} f^*(x | \mu_i) dx = \int_{x_0}^{\infty} \int f(x | \mu_i, \nu) \pi(\nu) d\nu dx \\ &= \int \left[\int_{x_0}^{\infty} f(x | \mu_i, \nu) dx \right] \pi(\nu) d\nu = \int p_i(\nu) \pi(\nu) d\nu \end{aligned} \quad (47)$$

(compare equation (36)), and the likelihood ratios become Bayes factors:

$$\lambda_{01} = \frac{f^*(x_0 | \mu_0)}{f^*(x_0 | \mu_1)} = \frac{\int f(x_0 | \mu_0, \nu) \pi(\nu) d\nu}{\int f(x_0 | \mu_1, \nu) \pi(\nu) d\nu}. \quad (48)$$

Although this approach lacks the frequentist error interpretation of the tests, it still enjoys the evidential interpretation of the p -values and Bayes factors. It is also conceptually simpler and more elegant, as well as computationally much easier, than the bootstrap.

8 Conclusion

We find that (p_0, p_1) plots such as figs. 5, 10 and 11 provide useful insights into several diverse statistical aspects of searches for new physics:

- The CL_s criterion for excluding H_1 ;
- The Punzi definition of sensitivity;
- The relationship between p -values and likelihoods;
- The difference between the exclusion regions using p -values and likelihoods;
- The probabilities of misleading evidence;
- The Jeffreys-Lindley paradox.

In addition, we believe that these plots could be helpful in summarizing the results of such searches. When these involve many channels, with possibly different sensitivities, one could plot the results as points on a (p_0, p_1) plot, together with Gaussian likelihood-ratio contours (since the latter are large-sample limits of the actual data pdf's). This would provide a convenient graphical overview of both the p -value and the likelihood-ratio evidence contained in the ensemble of channels investigated.

9 Acknowledgments

We are very grateful to Sir David Cox for insights into the Jeffreys-Lindley paradox, and to Bob Cousins for interesting discussions about it.

References

- [1] L. Lyons, “Raster scan or 2-D approach?,” [arXiv:1404.7395 \[hep-ex\]](#) (2014). 1
- [2] The use of two significances (one under the null and the other under the alternative hypothesis) as a system for assessing evidence is discussed in: Bill Thompson, “The nature of statistical evidence,” *Lecture notes in statistics 189*, Springer Science+Business Media, LLC, 2007, 152pp. 1
- [3] R. B. D’Agostino and M. A. Stephens (editors), “Goodness-of-fit techniques,” Marcel Dekker, Inc., 1986, 563pp. 2
- [4] M. Williams, “How good are your fits? Unbinned, multivariate goodness-of-fit tests in high energy physics,” [JINST 5:P09004](#) (2010); [arXiv:1006.3019 \[hep-ex\]](#) (2010). 2
- [5] In the statistics literature, testing problems that allow a ‘no-decision region’ were considered, possibly for the first time, in: E. L. Lehmann, “A theory of some multiple decision problems. II,” *Ann. Math. Statist.* **28**, 547 (1957). 2
- [6] A. L. Read, “Presentation of search results: the CL_s technique,” *J. Phys. G* **28**, 2693 (2002). 4
- [7] G. Cowan, K. Cranmer, E. Gross, and O. Vitells, “Asymptotic formulae for likelihood-based tests of new physics,” *Eur. Phys. J. C* **71**, 1554 (2011). 7
- [8] G. Punzi, “Sensitivity of searches for new signals and its optimisation”, [arXiv:physics/0308063 \[physics.data-an\]](#) (2003). 7
- [9] T. Sellke, M. J. Bayarri and J. O. Berger, “Calibration of p -values for testing precise null hypotheses,” *Amer. Statist.* **55**, 62 (2001); <http://www.stat.duke.edu/~berger/papers/99-13.html>. 12
- [10] J. O. Berger, “A comparison of testing methodologies,” in *Proceedings of the PHYSTAT-LHC workshop on statistical issues for LHC physics*, CERN, Geneva, Switzerland, 27-29 June 2007, edited by H. B. Prosper, L. Lyons, and A. De Roeck, [CERN Yellow Report CERN-2008-001](#) (2008), pg. 8-19. 12
- [11] R. Royall, “On the probability of observing misleading statistical evidence,” with discussion, *J. Amer. Statist. Assoc.* **95**, 760 (2000). 13, 14, 22
- [12] I. J. Good, “Comment on ‘Bayesian interpretation of standard inference statements’ by J. W. Pratt,” *J. R. Statist. Soc. B* **27**, 169 (1965). 16
- [13] S. Berry and K. Viele, “A note on hypothesis testing with random sample sizes and its relationship to Bayes factors,” *J. Data Science* **6**, 75 (2008). 16
- [14] G. E. P. Box, “Sampling and Bayes’ inference in scientific modelling and robustness [with discussion],” *J. R. Statist. Soc. A* **143**, 383 (1980). 17

- [15] R. D. Cousins, “The Jeffreys-Lindley paradox and discovery criteria in high energy physics,” [arXiv:1310.3791v4 \[stat.ME\]](#), 28 Jun 2014. 18, 20
- [16] R. E. Kass and A. E. Raftery, “Bayes factors,” *J. Amer. Statist. Assoc.* **90**, 773 (1995). 18
- [17] D. Cox, private communication (2014). 19
- [18] L. Demortier, “P Values and Nuisance Parameters,” in *Proceedings of the PHYSTAT-LHC Workshop on Statistical Issues for LHC Physics*, CERN, Geneva, Switzerland, 27-29 June 2007, edited by H. B. Prosper, L. Lyons, and A. De Roeck, [CERN Yellow Report CERN-2008-001 \(2008\)](#), pg. 23-33. 20, 22
- [19] See for example D.A.S. Fraser and J. Rousseau, “Studentization and deriving accurate p -values,” *Biometrika* **95**, 1 (2008), and C.J. Lloyd, “Some non-asymptotic properties of parametric bootstrap P-values in discrete models,” *Electronic J. Statist.* **6**, 2449 (2012). 22

A The Bayes-CL_s connection

This appendix describes a sufficient condition for CL_s upper limits to agree with Bayesian upper limits.

Let $f(x | \mu)$ be a family of probability densities for the random variable X , indexed by the parameter μ , and consider the family of tests:

$$H_0[\mu^*] : \mu = \mu^* \quad \text{versus} \quad H_1[\mu^*] : \mu > \mu^*. \quad (49)$$

Suppose we observe $X = x_0$. If we have a prior $\pi(\mu)$ for μ under $H_1[\mu^*]$, the Bayesian evidence in favor of $H_1[\mu^*]$ is simply the marginal probability of x_0 under $H_1[\mu^*]$:

$$p(x_0 | H_1[\mu^*]) = \int_{\mu^*}^{+\infty} f(x_0 | \mu) \pi(\mu) d\mu. \quad (50)$$

Note that this probability is only correctly normalized if $\pi(\mu)$ is a proper prior. However, the argument that follows remains valid if $\pi(\mu)$ is improper. The p -value evidence against $H_0[\mu^*]$, when the alternative is $H_1[\mu^*]$, is:

$$p_0(\mu^*) = \int_{x_0}^{+\infty} f(x | \mu^*) dx = 1 - F(x_0 | \mu^*), \quad (51)$$

where $F(x | \mu)$ is the cumulative probability distribution of x . This p -value evidence against $H_0[\mu^*]$ increases as $1 - p_0(\mu^*)$ increases. Assume now that the Bayesian and frequentist evidences are equal for all μ^* values larger than some prespecified μ_0 :

$$p(x_0 | H_1[\mu^*]) = 1 - p_0(\mu^*), \quad \text{for all } \mu^* \geq \mu_0, \quad (52)$$

or:

$$\int_{\mu^*}^{+\infty} f(x_0 | \mu) \pi(\mu) d\mu = \int_{-\infty}^{x_0} f(x | \mu^*) dx, \quad \text{for all } \mu^* \geq \mu_0. \quad (53)$$

This condition is sufficient to obtain equality of CL_s and Bayesian upper limits on μ under $H_1[\mu_0]$. Indeed, the γ -credibility level upper limit μ_U on μ is the solution of:

$$\int_{\mu_0}^{\mu_U} p(\mu | x_0, H_1[\mu_0]) d\mu = \gamma, \quad (54)$$

where the integrand is the posterior density of μ under $H_1[\mu_0]$:

$$p(\mu | x_0, H_1[\mu_0]) = \frac{f(x_0 | \mu) \pi(\mu)}{\int_{\mu_0}^{+\infty} f(x_0 | \mu') \pi(\mu') d\mu'} = \frac{f(x_0 | \mu) \pi(\mu)}{p(x_0 | H_1[\mu_0])}. \quad (55)$$

Substituting equation (55) in (54) leads to:

$$\frac{p(x_0 | H_1[\mu_0]) - p(x_0 | H_1[\mu_U])}{p(x_0 | H_1[\mu_0])} = \gamma, \quad (56)$$

and using condition (52) yields:

$$1 - \frac{1 - p_0(\mu_U)}{1 - p_0(\mu_0)} = \gamma. \quad (57)$$

The quantity $1 - p_0(\mu_U)$ is in fact $p_1(\mu_U)$, the p -value for testing $\mu = \mu_U$ when the alternative is $\mu = \mu_0$. Hence, equation (57) is equivalent to

$$\frac{p_1(\mu_U)}{1 - p_0(\mu_0)} = 1 - \gamma, \quad (58)$$

which corresponds to the CL_s construction of upper limits.

We illustrate this result with two examples of families of distributions that satisfy condition (52). The first one is any family of continuous distributions parametrized by a location parameter:

$$f(x | \mu) = f(x - \mu). \quad (59)$$

It is straightforward to verify, by integration by substitution, that

$$\int_{-\infty}^x f(x' - \mu) dx' = \int_{\mu}^{+\infty} f(x - \mu') d\mu', \quad (60)$$

so that condition (52) is indeed satisfied for a flat prior, $\pi(\mu) = 1$. The second example is the Poisson family:

$$f(n | \mu) = \frac{\mu^n}{n!} e^{-\mu}, \quad (61)$$

for which we have:

$$\sum_{i=0}^n \frac{\mu^i}{i!} e^{-\mu} = \int_{\mu}^{+\infty} \frac{t^n}{n!} e^{-t} dt, \quad (62)$$

as can be checked by repeated integration by parts of the right-hand side. Although this is a discrete version of condition (52), also with a flat prior, nothing essential changes in the argument leading from (54) to (58).

B Figures

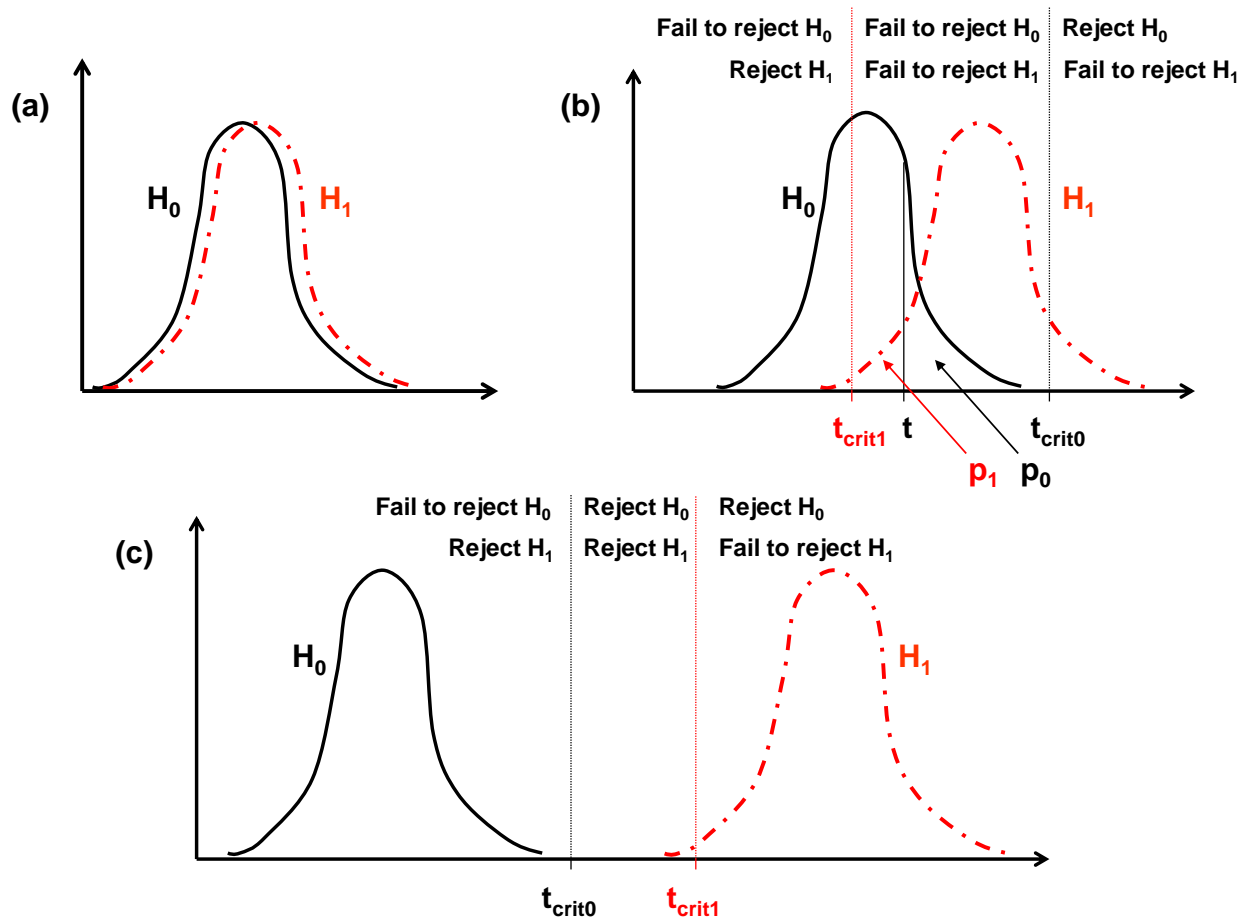


Figure 1: Probability density functions (pdf's) of a test statistic T under two hypotheses H_0 (solid) and H_1 (dot-dashed). In (a) the separation of the pdf's is small, making the two hypotheses almost indistinguishable. The separation in (b) is such that the data can exclude H_1 , reject neither H_0 nor H_1 , or reject H_0 . Given an observed value t of the test statistic T , diagram (b) illustrates the definitions of p_0 and p_1 : p_0 is the tail area under H_0 in the direction of H_1 , whereas p_1 is the tail area under H_1 in the direction of H_0 . The quantities t_{crit0} and t_{crit1} are the critical values of T , beyond which the data are considered incompatible with H_0 and H_1 respectively; the value of p_0 at $T = t_{crit0}$ is α_0 . The p_1 value at this value of T is denoted by β_0 . In (c) the pdf's are far apart and the observed value of T will always reject at least one hypothesis.

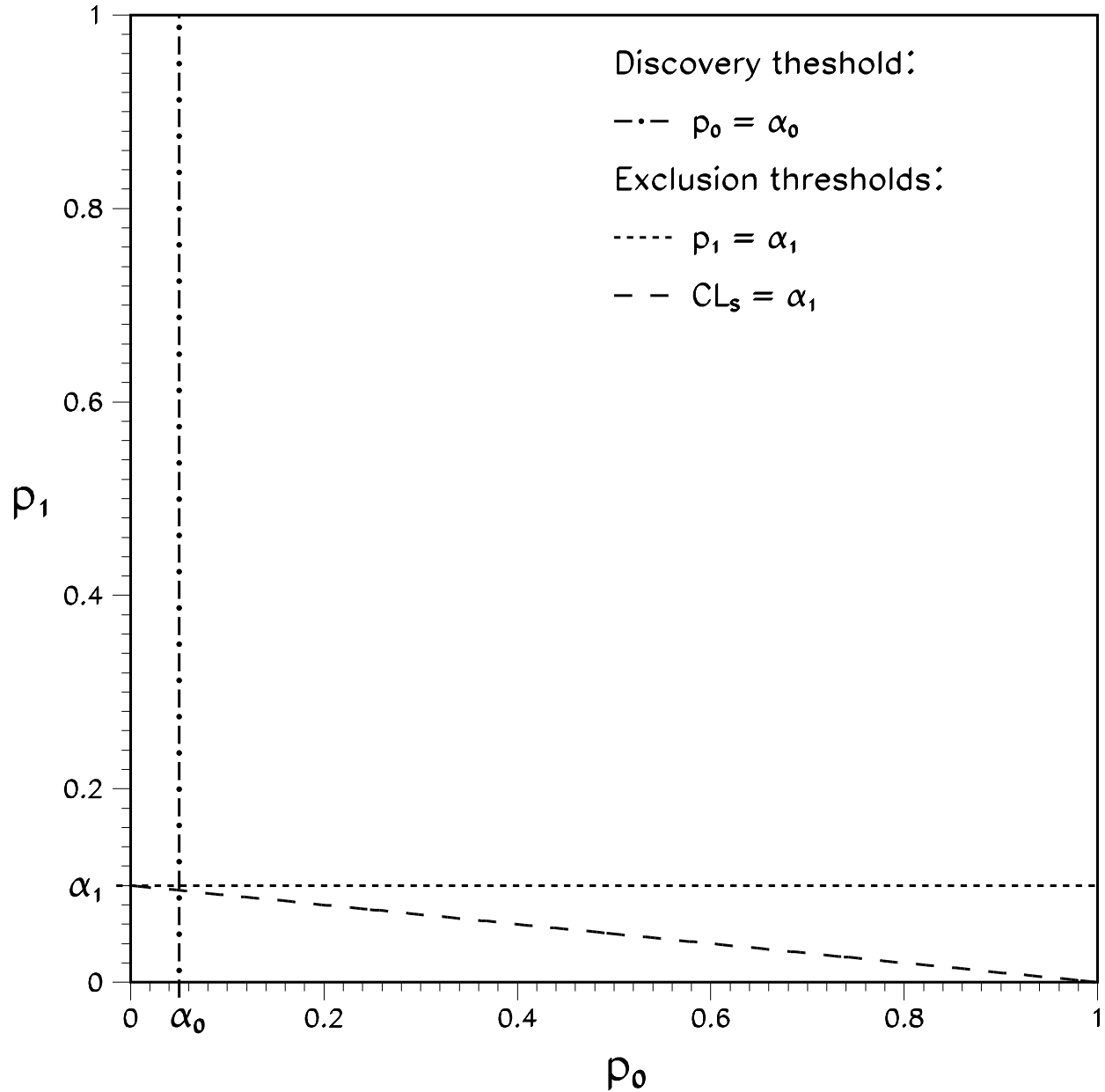


Figure 2: Plot of p_0 versus p_1 with three lines: The vertical line at $p_0 = \alpha_0$ is an example of a cut used for rejecting H_0 when p_0 is small. Correspondingly, the horizontal line at $p_1 = \alpha_1$ could be used for excluding H_1 when p_1 is small (less than 10% in the figure). If the observed value of the test statistic T was such that (p_0, p_1) was in the large rectangle, the data would be consistent with both hypotheses, while for the small rectangle near the origin, it would be inconsistent with both. An alternative procedure for excluding H_1 is based on $CL_s = p_1/(1 - p_0)$, and requires (p_0, p_1) to be below the sloping line.

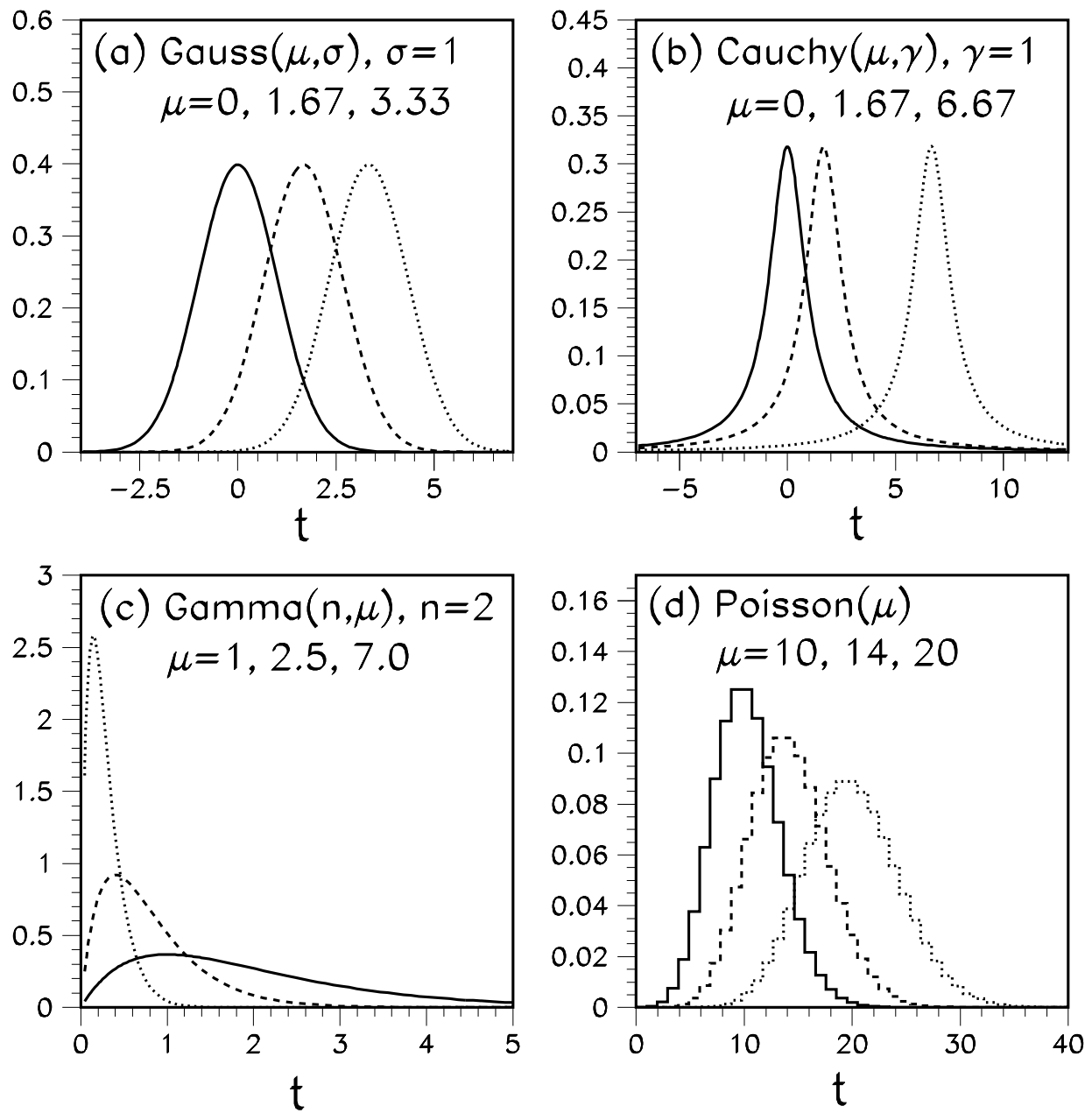


Figure 3: Probability densities (plots a, b, and c) and probabilities (plot d) used to draw fixed-hypothesis contours on figure 4.

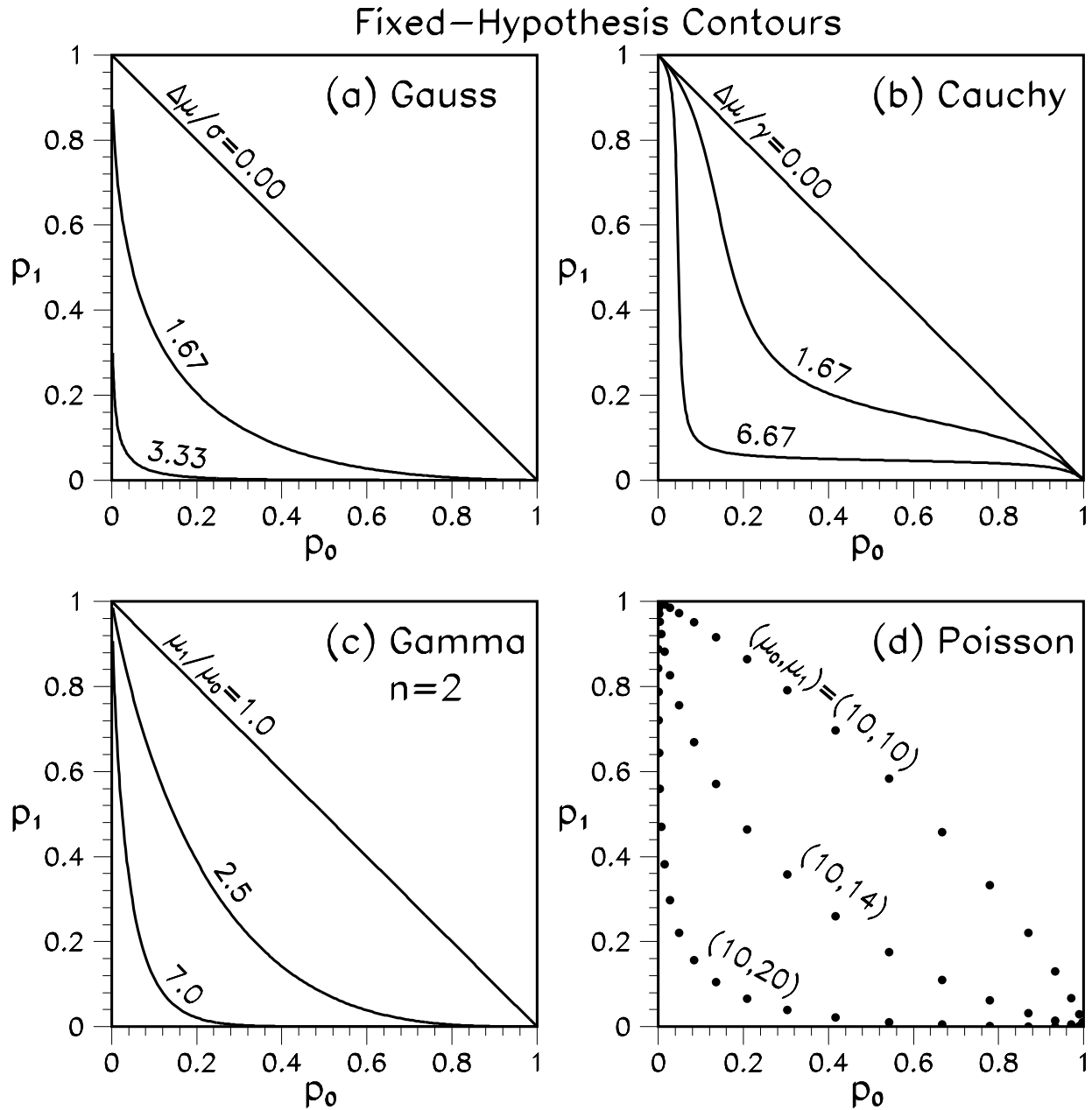


Figure 4: Fixed-hypothesis contours in the p_0 versus p_1 plane for four different choices of pdf: (a) Gauss, (b) Cauchy, (c) Gamma, and (d) Poisson. In each case one is testing $H_0 : \mu = \mu_0$ versus $H_1 : \mu = \mu_1$ where μ is the mean of the distribution (or mode, in the case of Cauchy). In the Gauss, Cauchy, and Gamma cases, the contours depend on a simple combination of μ_0 and μ_1 , but not on their individual values. The line $p_1 = 1 - p_0$ is an upper boundary for observable p -values in plots (a), (b), and (c), but not in the discrete Poisson case of plot (d).

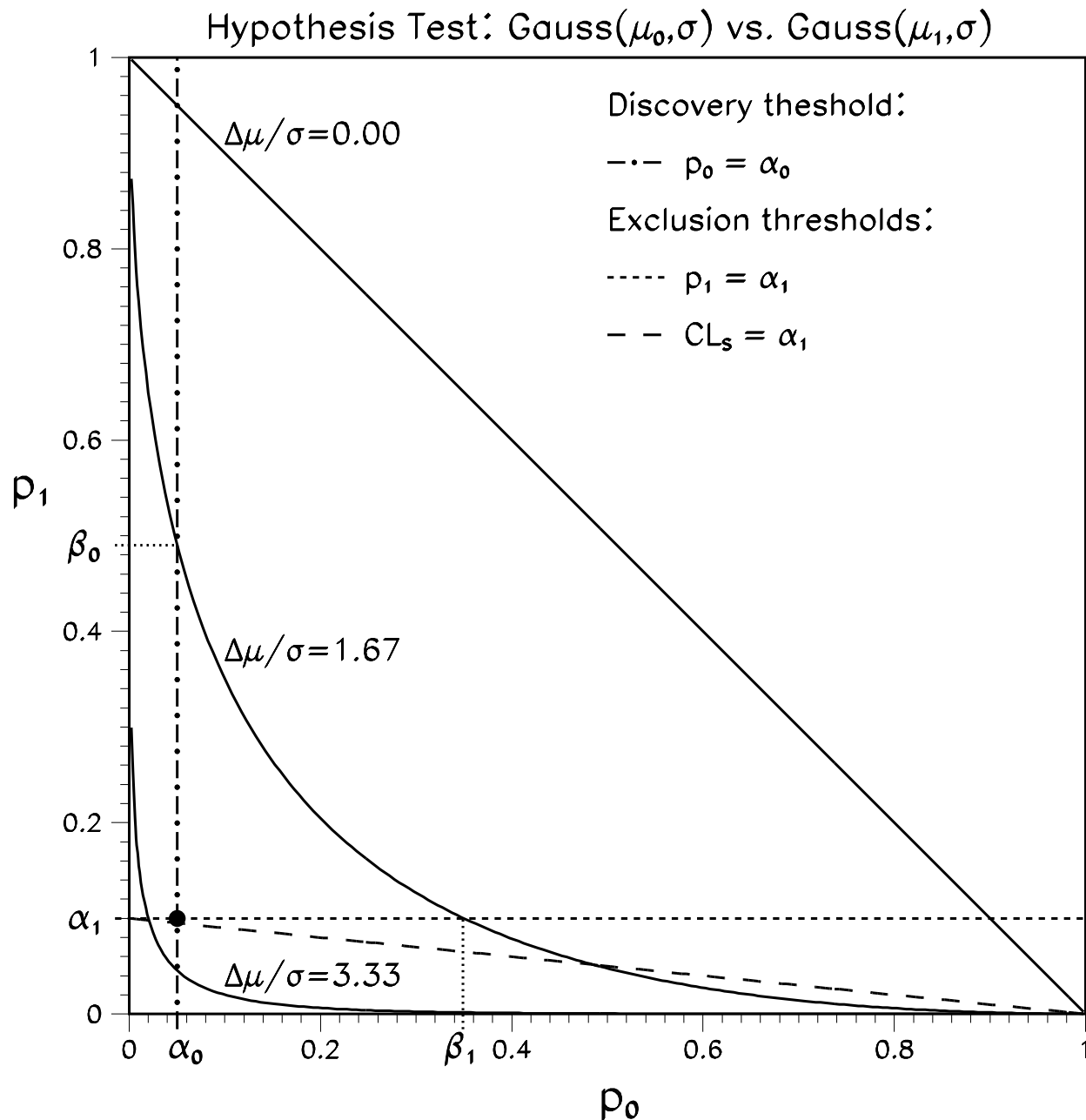


Figure 5: Plot of p_0 versus p_1 with fixed-hypothesis contour lines, as in figure 4(a). For fixed pdf's under H_0 and H_1 , the possible values of the test statistic T correspond to a curve in the (p_0, p_1) plane. The examples shown are for Gaussian pdf's where $\Delta\mu/\sigma$ is zero (i.e., identical pdf's under H_0 and H_1), 1.67 and 3.33. When $\Delta\mu/\sigma = 3.33$, the separation of the pdf's is large enough that the data cannot fall in the large no-decision region, defined by $p_0 > \alpha_0$ & $p_1 > \alpha_1$. We refer to the black dot at the intersection of the horizontal dashed and vertical dot-dashed lines as the 'Punzi point' (see text). For a given choice of α_0 , the intersection of the line $p_0 = \alpha_0$ with the relevant contour has ordinate β_0 , the probability of failing to reject H_0 when H_1 is true (the plot shows this for the $\Delta\mu/\sigma = 1.67$ contour). The relation between α_1 and β_1 is similar.

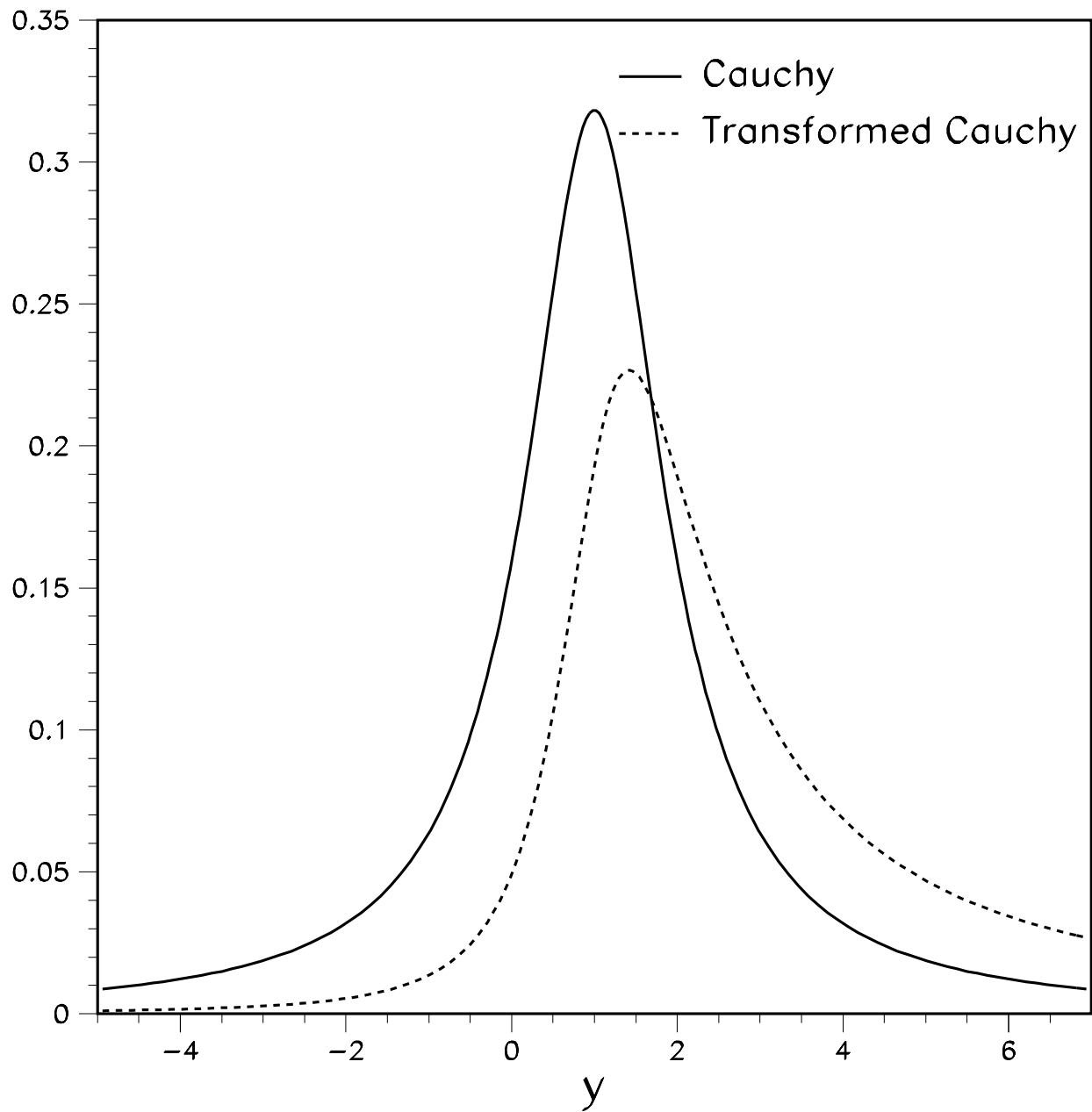


Figure 6: Solid line: Cauchy probability density function with mode μ_c and scale parameter γ both equal to 1. Dashed line: asymmetric pdf obtained by a one-to-one transformation of the Cauchy density (see equation (14) in the text, with $\mu_c = \gamma = \Delta\mu/\sigma = 1$).

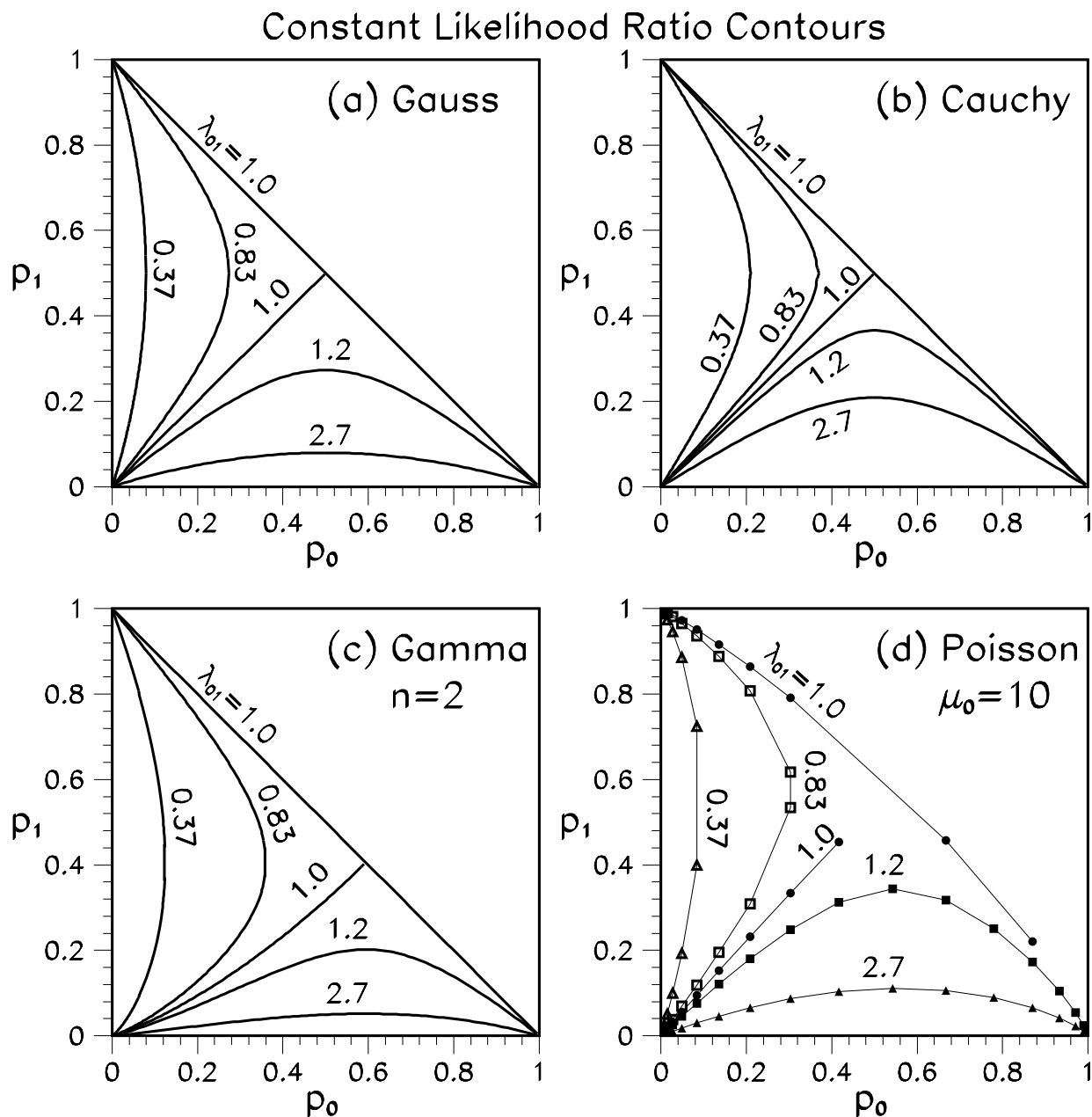


Figure 7: Contours of constant likelihood ratio $\lambda_{01} \equiv L_0/L_1$ in the p_0 versus p_1 plane for four different choices of pdf: (a) Gauss, (b) Cauchy, (c) Gamma, and (d) Poisson, where the lines merely join up the discrete (p_0, p_1) points as “contours”. In each case one is testing $H_0 : \mu = \mu_0$ versus $H_1 : \mu = \mu_1$ where μ is the pdf mean for Gauss and Poisson, mode for Cauchy, and rate parameter for Gamma. To facilitate comparison, the same contours are drawn in all four cases. In plot (d), points line up vertically across contours, since by construction μ_0 is the same everywhere.

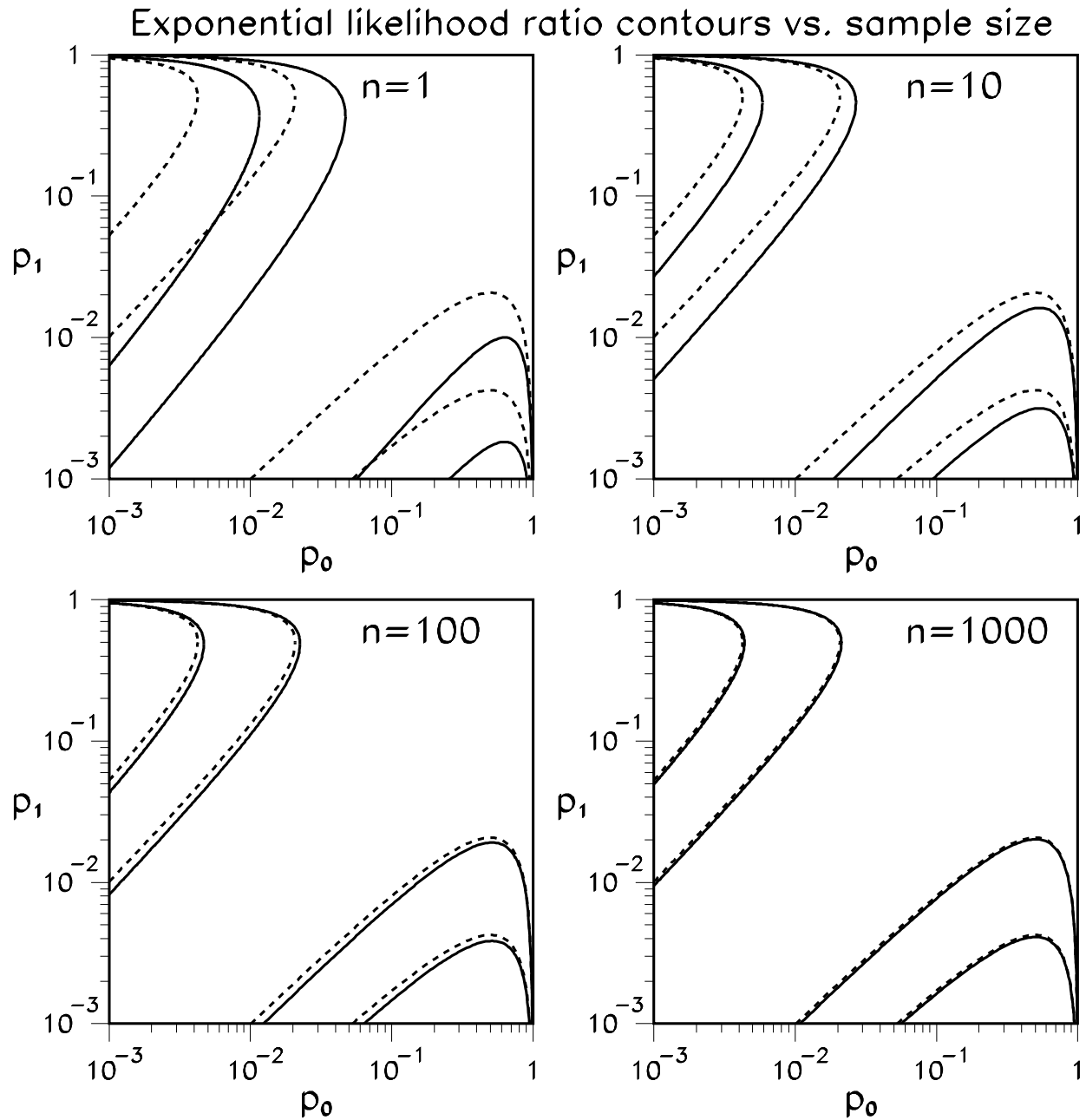


Figure 8: Likelihood-ratio contours for testing the value of an exponential decay rate for four different values of the number n of decay time measurements included in the test (solid lines), compared with the corresponding contours for a Gaussian test (dashed lines). At large n , the exponential contours converge to the Gaussian ones. From left to right in each plot, the contours correspond to $\lambda_{01} = 1/32, 1/8, 8,$ and 32 .

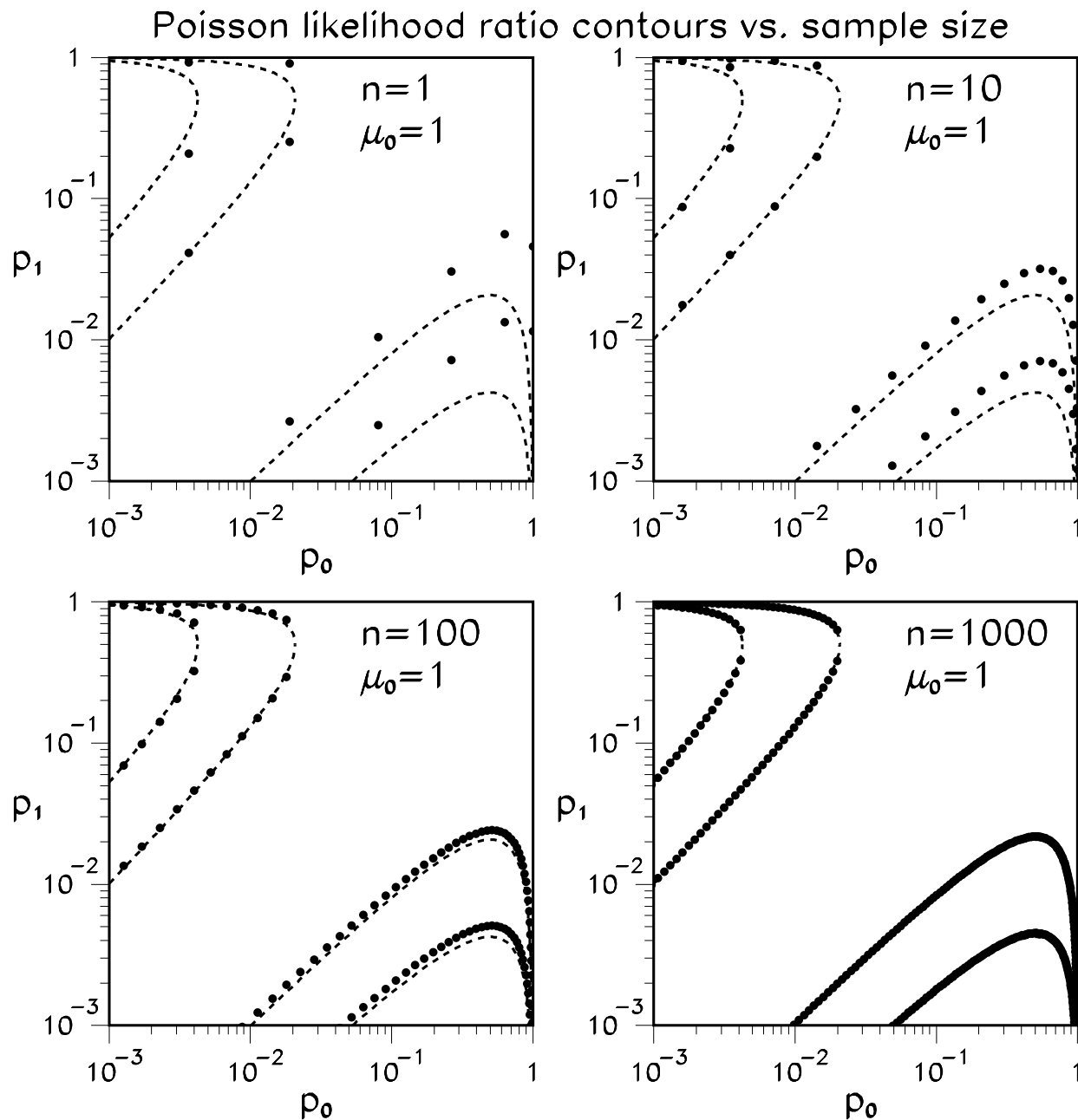


Figure 9: Likelihood-ratio contours for testing the value of a Poisson mean for four different values of the number n of measurements included in the test (dots), compared with the corresponding contours for a Gaussian test (dashed lines). At large n , the Poisson contours converge to the Gaussian ones. From left to right in each plot, the contours correspond to $\lambda_{01} = 1/32, 1/8, 8, \text{ and } 32$.

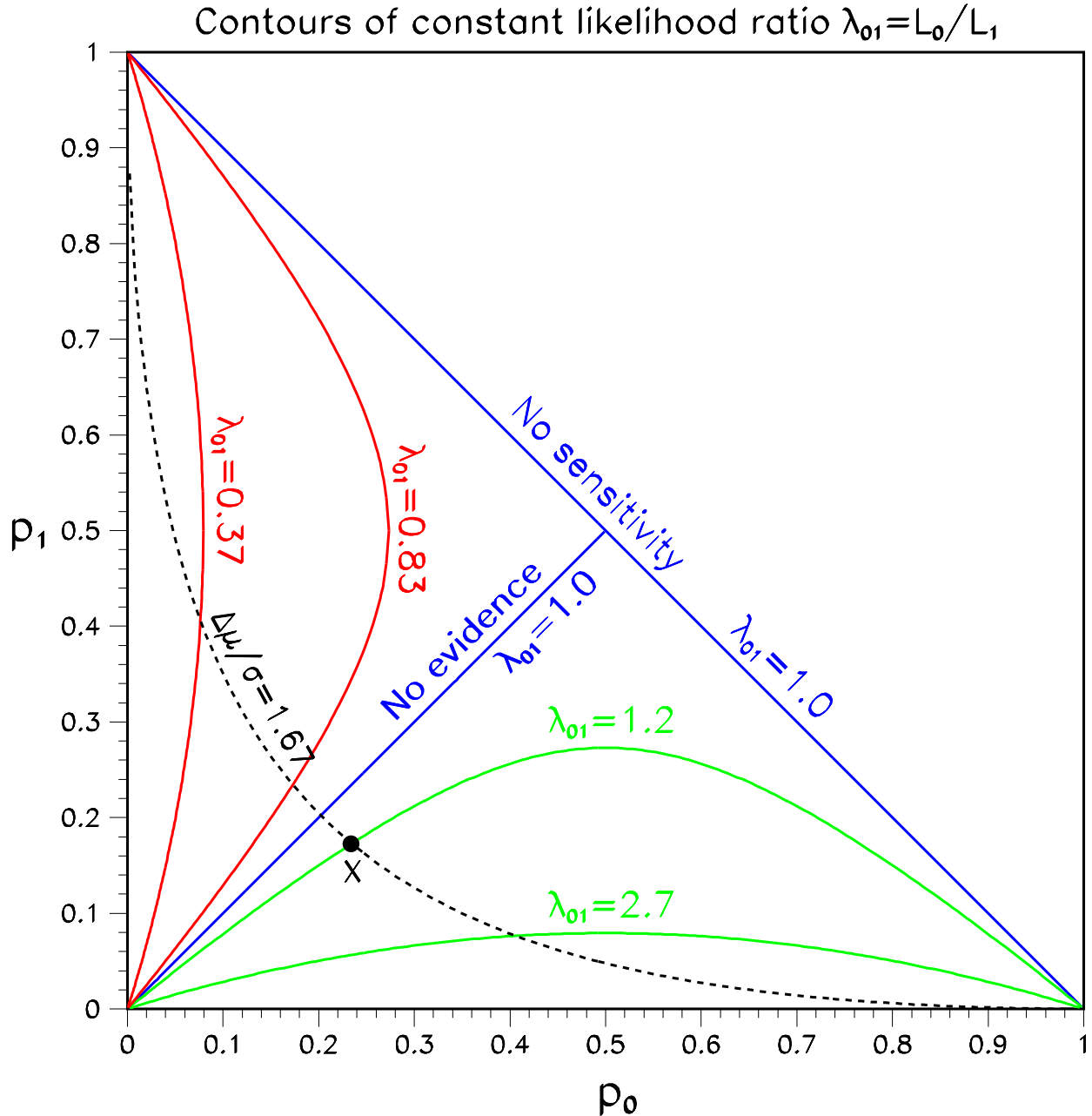


Figure 10: Plot of p_0 versus p_1 with likelihood ratio contours (colored, solid lines), when the pdf's are Gaussians of equal width. The likelihood ratio is unity along the $p_1 = 1 - p_0$ diagonal, where H_1 is identical to H_0 , and along the $p_1 = p_0$ diagonal, where the observed value of the test statistic favors each hypothesis equally. Going down a line of constant p_0 from $p_1 = 0.5$ to $p_1 = 0$ corresponds to increasing separation of the pdf's (e.g., more and more data), and also to increasing L_0/L_1 . This gives rise to the possibility of p_0 being small while L_0/L_1 is large. In fact one could exclude H_0 or H_1 based on the observed likelihood ratio instead of p_0 or p_1 ; the corresponding exclusion regions have a different shape from the p -value exclusion regions. The dashed line is a contour of constant $\Delta\mu/\sigma$. Its intersections with likelihood-ratio contours provides various probabilities of misleading evidence (see text).

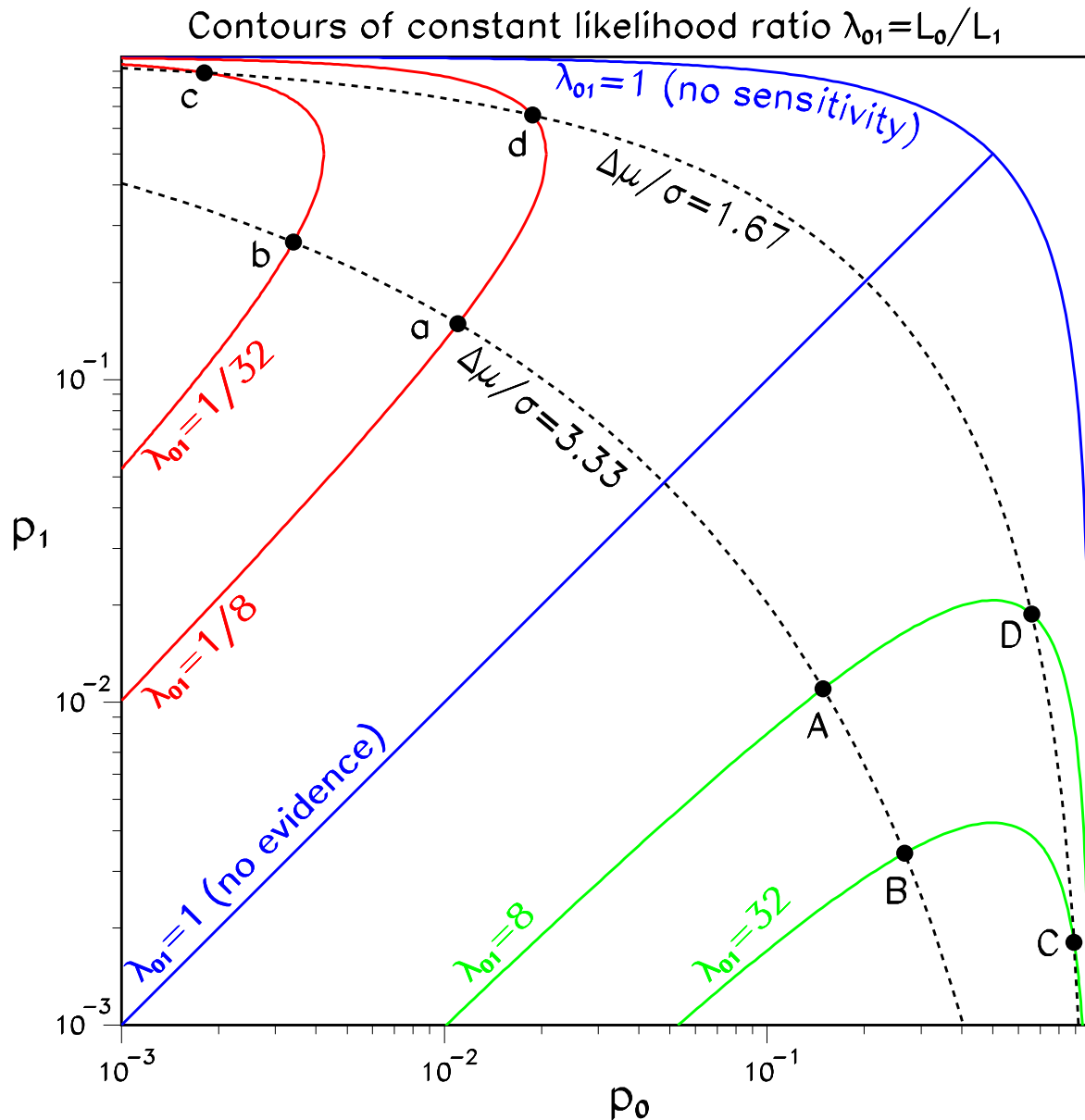


Figure 11: Log-log version of the plot of p_0 versus p_1 , assuming that the pdf's of the test statistic under H_0 and H_1 are Gaussian with the same width. Solid lines show the likelihood-ratio contours for $L_0/L_1 = 1/32, 1/8, 1, 8$ and 32 , and dashed lines show the fixed-hypothesis contours for $\Delta\mu/\sigma = 1.67$ and 3.33 . The p_0 coordinates of points a, b, c and d , and the p_1 coordinates of points A, B, C and D yield the probabilities of misleading evidence listed in the table below.

$\Delta\mu/\sigma$	1.67	3.33
$\mathbb{P}(L_0/L_1 < 1/32 \mid H_0)$	0.18%	0.34%
$\mathbb{P}(L_0/L_1 < 1/8 \mid H_0)$	1.9%	1.1%
$\mathbb{P}(L_0/L_1 > 8 \mid H_1)$	1.9%	1.1%
$\mathbb{P}(L_0/L_1 > 32 \mid H_1)$	0.18%	0.34%

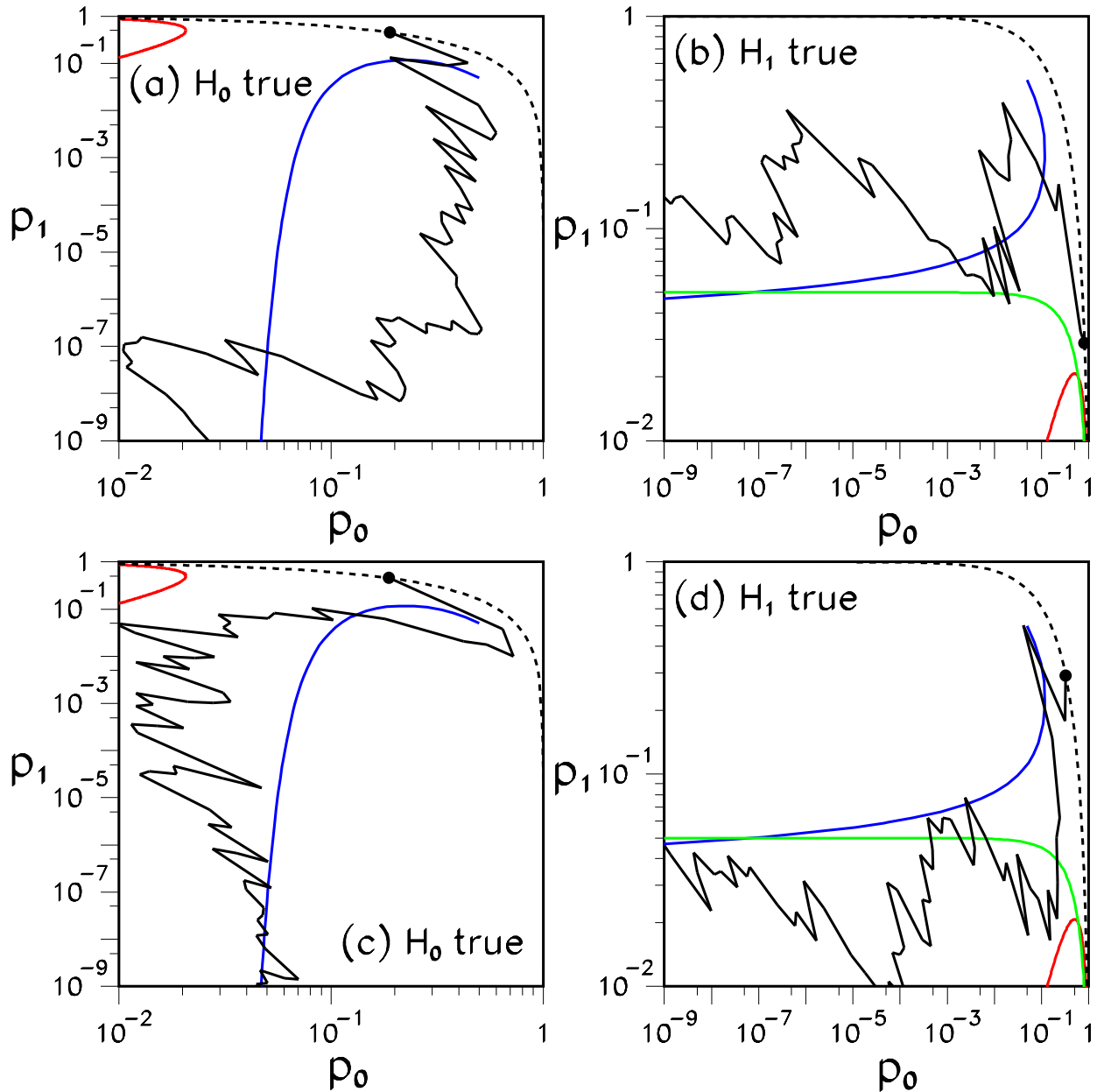
Sequential testing under H_0 and under H_1 

Figure 12: Four examples of sequential testing on the mean of a Gaussian distribution with unit width. Plots (a) and (c) assume that H_0 is true, whereas plots (b) and (d) assume the truth of H_1 . A sequential testing procedure (see text) describes a random walk in the (p_0, p_1) plane (shown by the black broken lines). The blue curves represent the boundary defined by the law of the iterated logarithm (LIL). The red likelihood-ratio contours (for $\lambda_{01} = 1/8$ in plots (a) and (c), and for $\lambda_{01} = 8$ in plots (b) and (d)) are examples of decision boundaries that avoid the possibility of testing to a foregone conclusion implied by the LIL. The green line in plots (b) and (d) represents the $CL_s = 5\%$ decision boundary, which does not avoid this possibility.

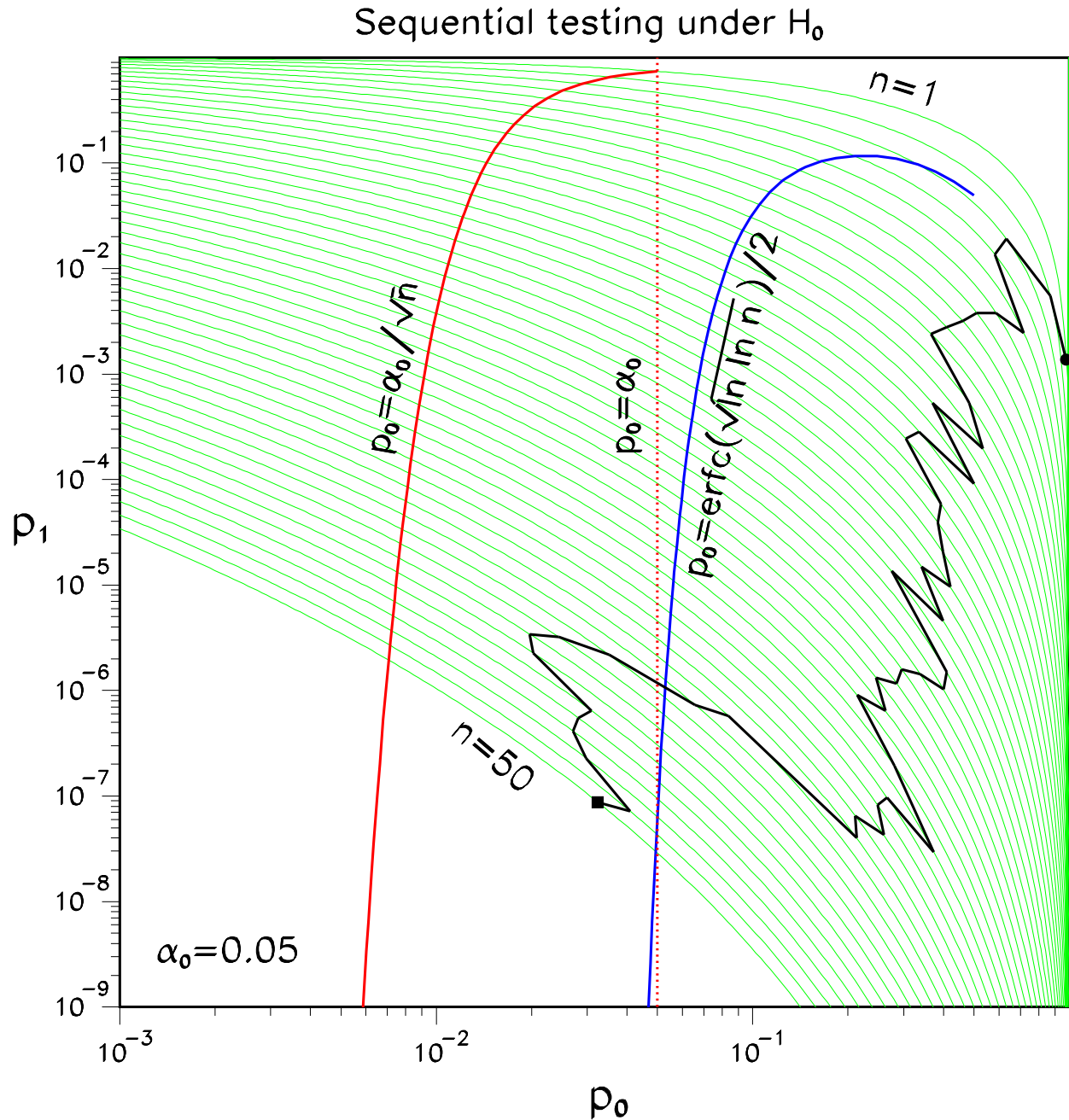


Figure 13: Plot showing fifty fixed-hypothesis contours (green curves) crossed by a random walk (black broken line) associated with a sequential test procedure of the Gauss(μ_0, σ) versus Gauss(μ_1, σ) type. At each step the sample size n increases by one, and the walk moves to a contour with improved resolution. Contours are labeled by the value of n . The blue curve shows the relationship between p_0 and n described by the LIL boundary. The red dotted line represents a fixed discovery threshold α_0 . Since this line crosses to the large- p_0 side of the LIL boundary, it is guaranteed to have the pathology of sampling to a foregone conclusion. In contrast, with the p_0 cutoff set as α_0/\sqrt{n} (solid red line), repeated sampling does not necessarily lead to exclusion of a true H_0 .

Explanation of the Jeffreys–Lindley paradox

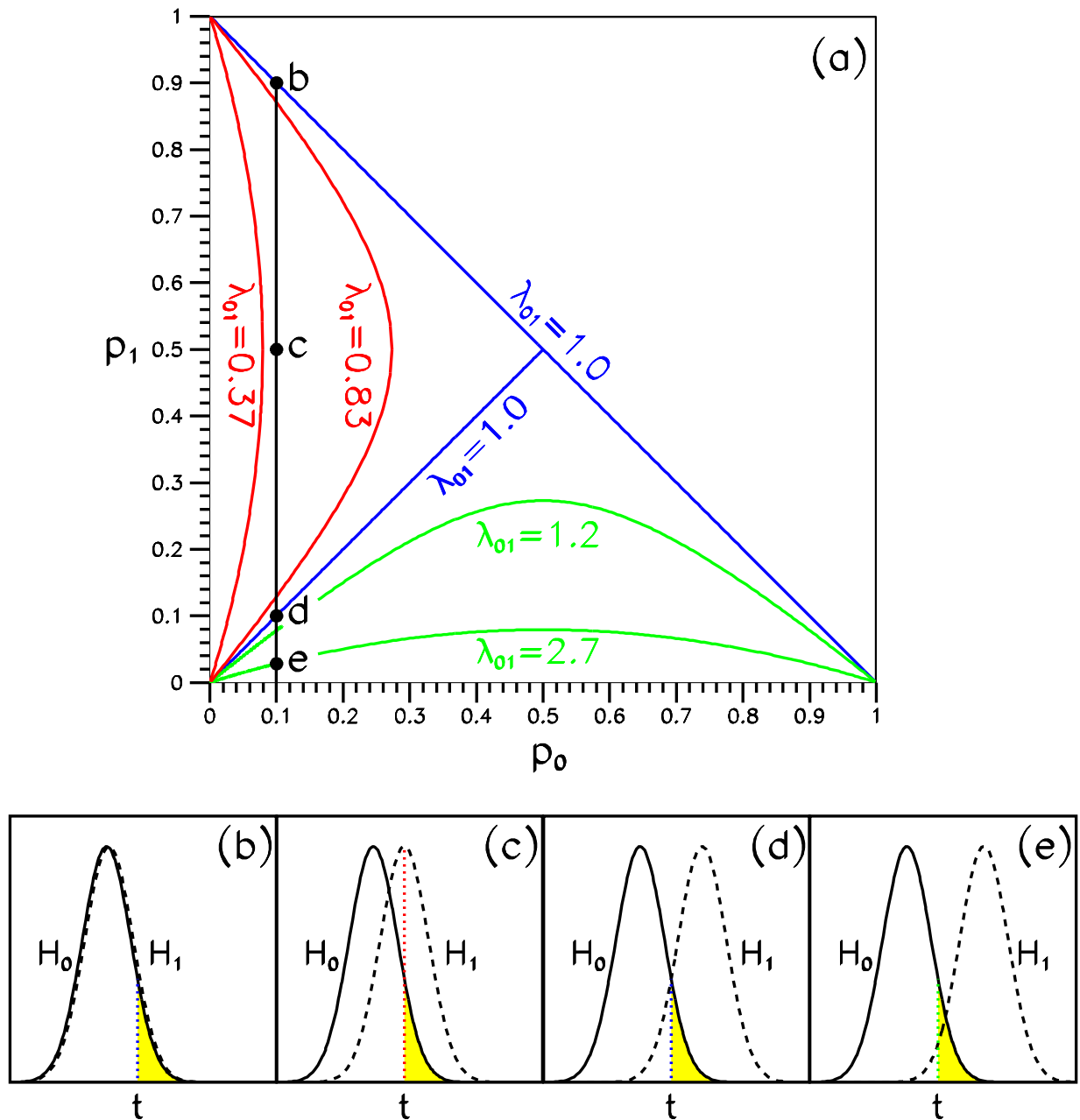


Figure 14: Insight for the Jeffreys-Lindley paradox. The likelihood ratio contours in (a) are those of figure 7(a) for comparing hypotheses whose pdf's are equal-width Gaussians. The line $bcd e$ is at fixed p_0 , with the points b to e corresponding to increasing separation of the H_0 and H_1 pdf's, as shown in diagrams (b) to (e) respectively.

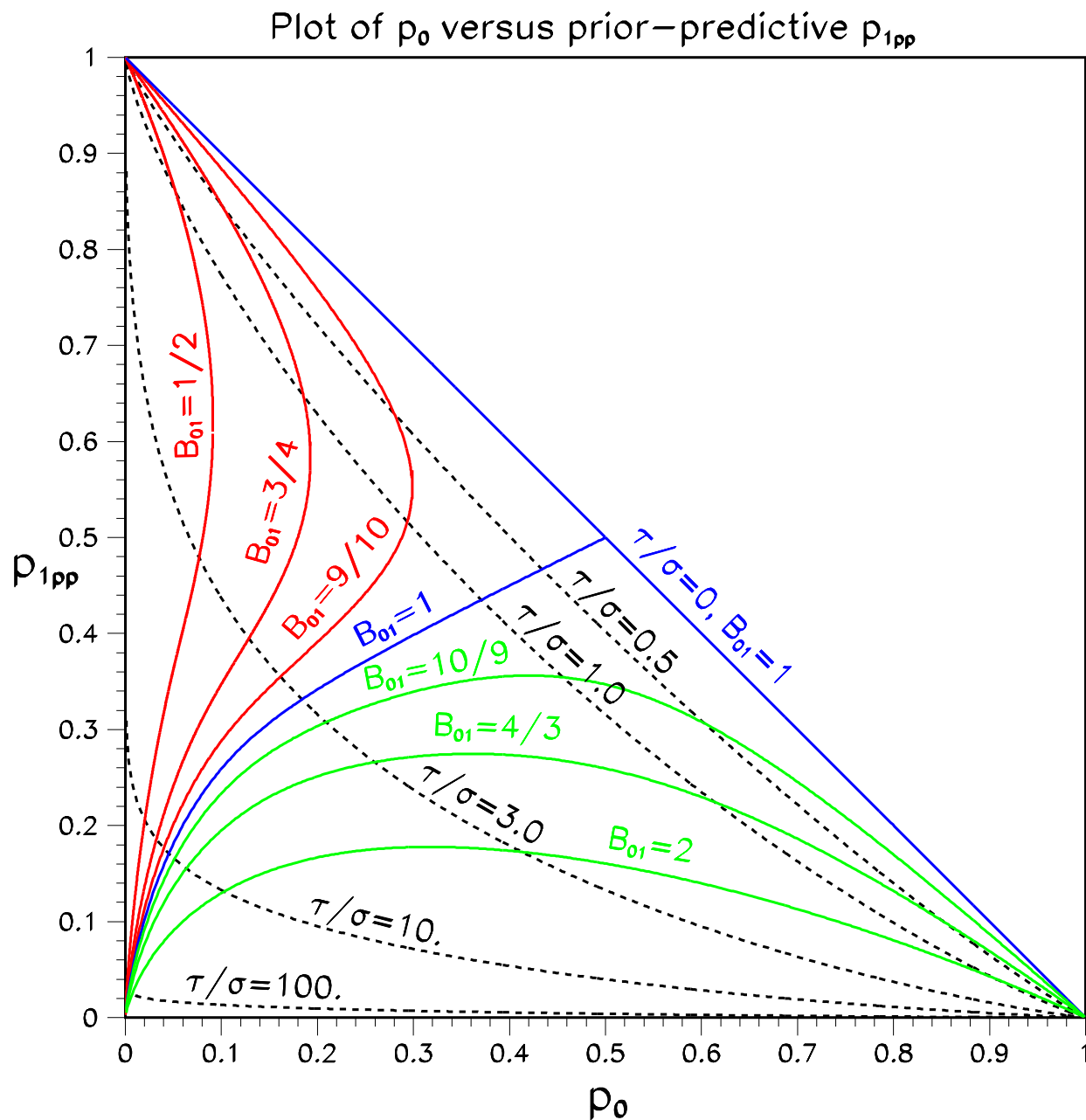


Figure 15: Plot of p_0 versus prior-predictive p_1 for testing $H_0 : \mu = \mu_0$ versus $H_1 : \mu > \mu_0$. The test statistic has a Gaussian distribution with mean μ and standard deviation σ . The prior for μ under H_1 equals $1/\tau$ for $\mu_0 < \mu \leq \mu_0 + \tau$ and is zero otherwise. Fixed-hypothesis contours (dashed lines) are labeled by the value of τ/σ . Constant Bayes factor contours (colored solid lines) are also shown.

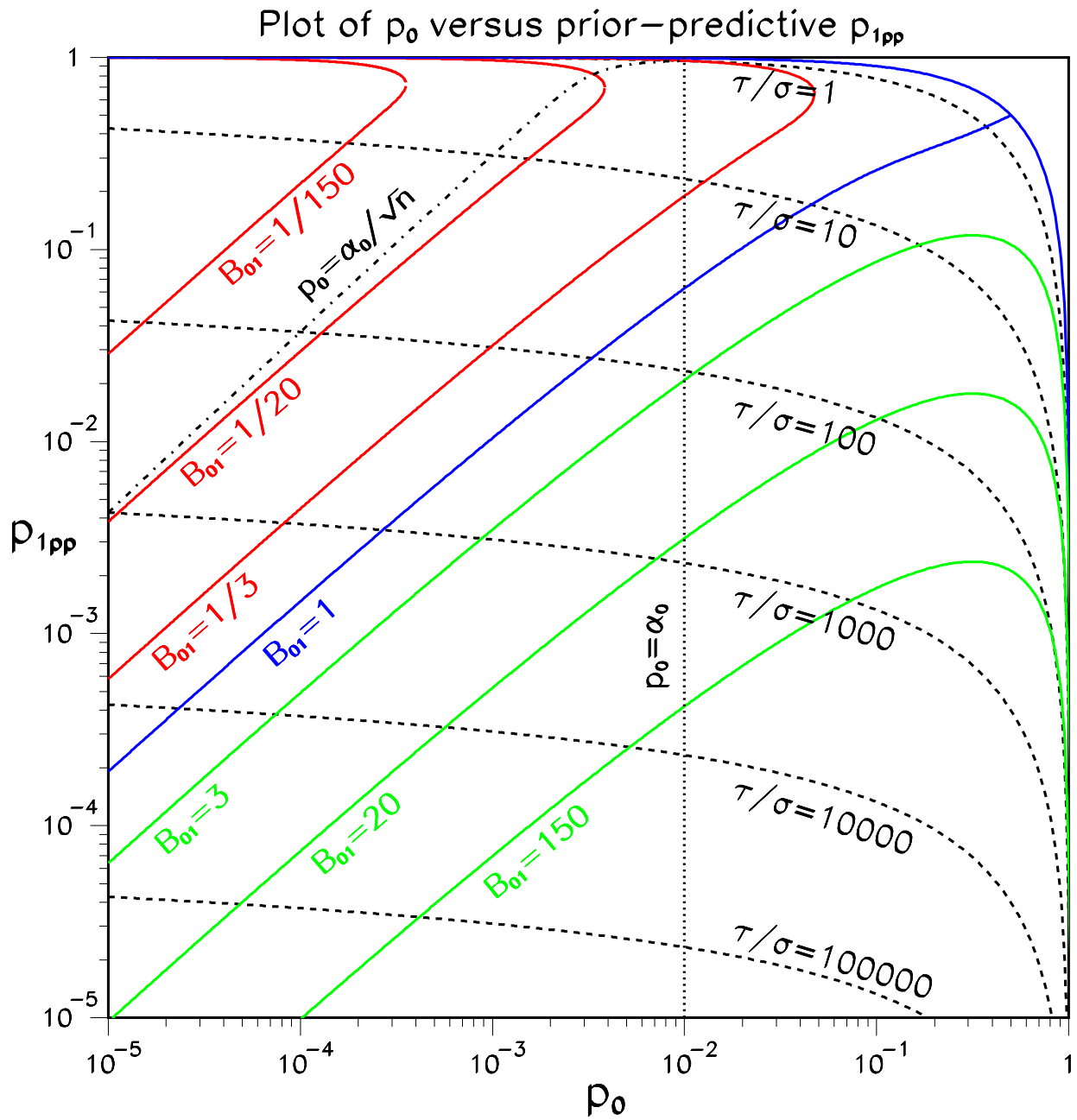


Figure 16: Log-log version of figure 15, with a larger range of fixed-hypothesis contours and more realistic values for the Bayes factor contours. Also shown are the constant p_0 threshold (dotted line) at $\alpha_0 = 1\%$ and the corresponding n -dependent threshold α_0/\sqrt{n} (dot-dashed line), where n is the sample size.

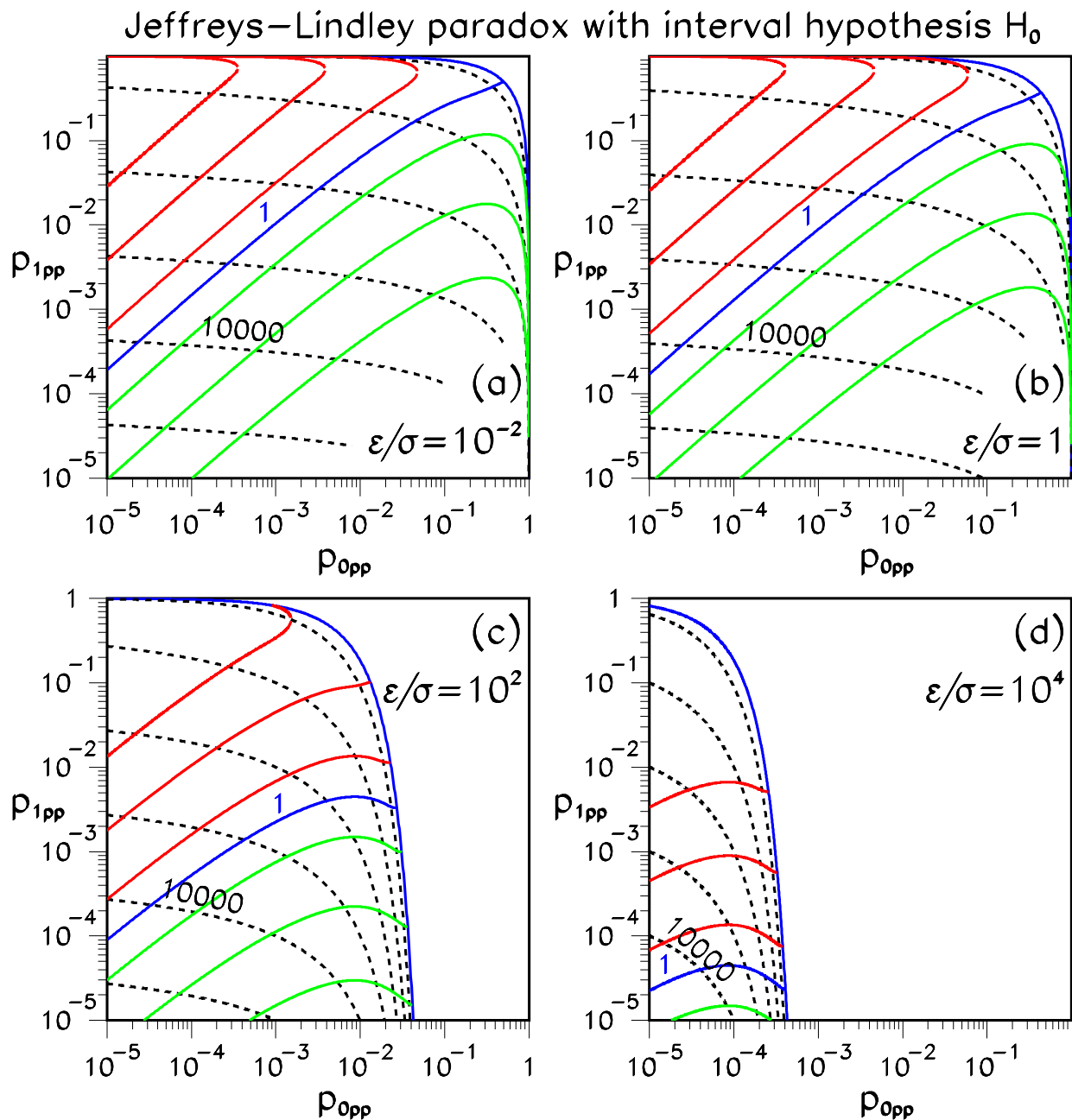


Figure 17: Plots illustrating what happens to the Jeffreys-Lindley paradox when H_0 is an interval hypothesis with width ϵ instead of a point-null hypothesis. Both p_{0pp} and p_{1pp} are prior-predictive p -values. The contours on these plots are the same as in figure 16, although for clarity only the contours $\tau/\sigma = 10000$ and $B_{01} = 1$ are labeled. Compared with figure 16, the fixed-hypothesis contours and the constant Bayes factor contours are both changed in such a way that the paradox remains present regardless of the value of ϵ/σ .

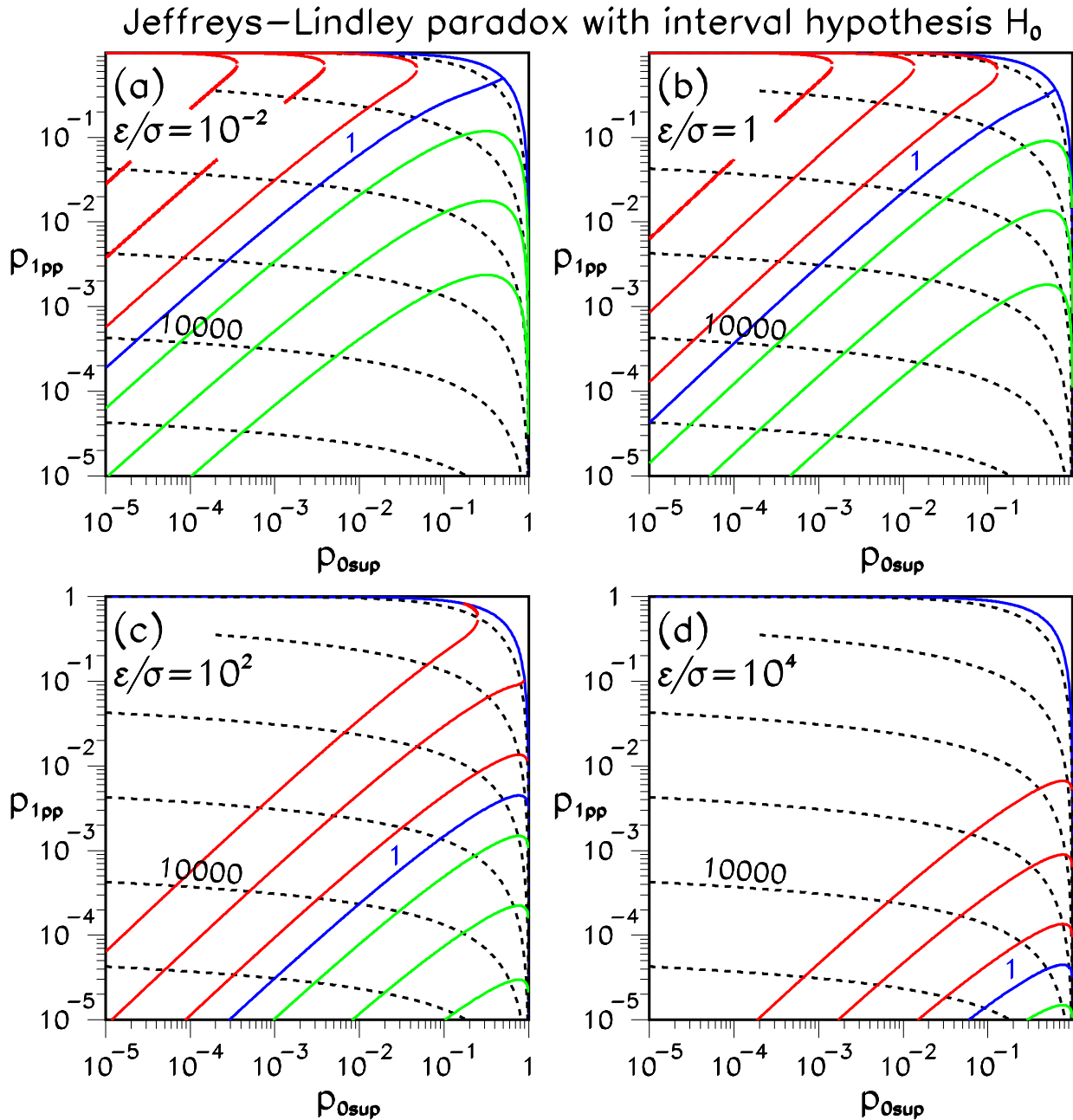


Figure 18: Plots illustrating what happens to the Jeffreys-Lindley paradox when H_0 is an interval hypothesis with width ϵ instead of a point-null hypothesis. The p -value p_{1pp} is a prior-predictive p -value, whereas p_{0sup} is a supremum p -value. The contours on these plots are the same as in figure 16, although for clarity only the contours $\tau/\sigma = 10000$ and $B_{01} = 1$ are labeled. Compared with figure 16, only the constant Bayes factor contours are changed; the fixed-hypothesis contours are the same. The result is that the paradox disappears for a suitably high value of ϵ/σ .

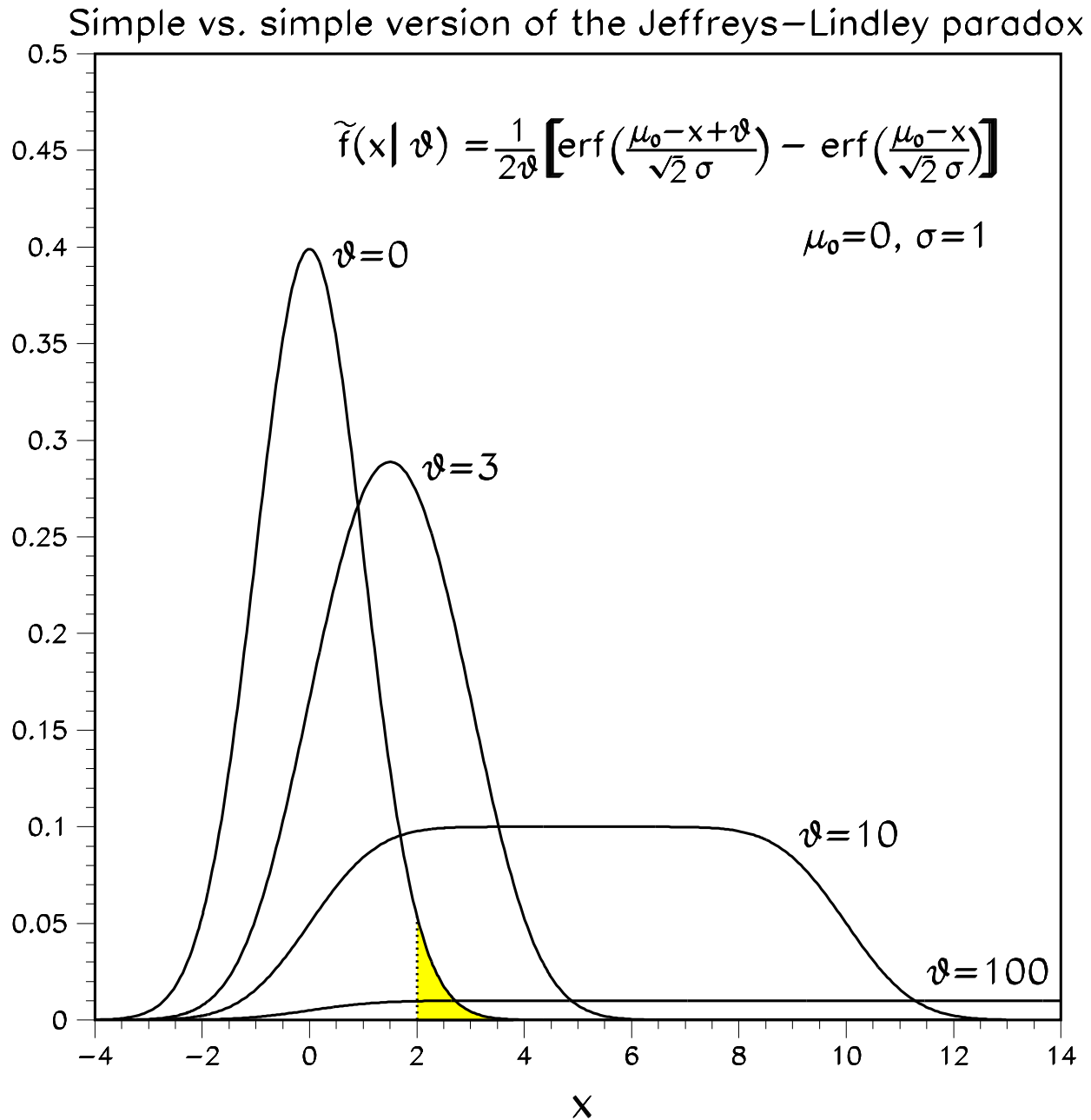


Figure 19: Plot of the integrated pdf (44) for several values of the parameter θ (the pdf for $\theta = 100$ has been truncated at the upper end). If for example $x = 2$ is observed, the p -value under $H_0 : \theta = 0$ is 2.3% (shaded area), but the likelihood ratio of $\theta = 0$ to $\theta = 100$ is 5.5. It is clear that for very large θ values, significantly small p -values that disfavor H_0 will be associated with likelihood ratios that favor H_0 . This is a simple versus simple version of the Jeffreys-Lindley paradox.